Variations in Monthly Maximum Gust Speed at St Mary's, Isles of Scilly (UK)

Masina, Marinella ; D'Ayala, Dina; Antonini, Alessandro

DOI
10.1029/2022EA002380

Publication date
2022

Document Version
Final published version

Published in
Earth and Space Science

Citation (APA)
Masina, M., D'Ayala, D., & Antonini, A. (2022). Variations in Monthly Maximum Gust Speed at St Mary's, Isles of Scilly (UK). *Earth and Space Science*, *9*(11), Article e2022EA002380. https://doi.org/10.1029/2022EA002380

Earth and Space Science

RESEARCH ARTICLE
10.1029/2022EA002380

Variations in Monthly Maximum Gust Speed at St Mary's, Isles of Scilly (UK)

Marinella Masina[1,2], Dina D'Ayala[3], and Alessandro Antonini[1]

[1]Department of Hydraulic Engineering, Delft University of Technology, Delft, The Netherlands, [2]Now at Interdepartmental Centre for Industrial Agrofood Research (CIRI Agrofood), University of Bologna, Cesena, Italy, [3]Department of Civil, Environmental and Geomatic Engineering, University College London, London, UK

Key Points:

- Homogenization of historical gust speeds at St Mary's, Isles of Scilly, has been performed to remove discontinuities caused by non-climatic changes
- Summer gust speeds have significantly increased, while winter gust speeds have declined in 1969–2011 and strengthened since 2012
- Statistically significant correlations are found between monthly maximum gust speeds and main climate indices which might explain the observed variability

Correspondence to:
A. Antonini,
A.Antonini@tudelft.nl

Citation:
Masina, M., D'Ayala, D., & Antonini, A. (2022). Variations in monthly maximum gust speed at St Mary's, Isles of Scilly (UK). *Earth and Space Science*, *9*, e2022EA002380. https://doi.org/10.1029/2022EA002380

Received 21 APR 2022
Accepted 20 OCT 2022

Author Contributions:
Conceptualization: Marinella Masina, Alessandro Antonini
Data curation: Marinella Masina
Formal analysis: Marinella Masina
Funding acquisition: Dina D'Ayala, Alessandro Antonini
Investigation: Marinella Masina
Methodology: Marinella Masina
Software: Marinella Masina
Supervision: Alessandro Antonini
Writing – original draft: Marinella Masina
Writing – review & editing: Marinella Masina, Dina D'Ayala, Alessandro Antonini

Abstract Long-term variations in maximum gust speeds have been analyzed using wind measurements recorded at St Mary's, Isles of Scilly, UK, and possible drivers of recent changes have been investigated. A rigorous homogenization procedure has been applied to the wind records to remove discontinuities mainly caused by non-climatic changes. Trends in magnitude of the homogenized annual and monthly maximum gust speeds have been subsequently estimated. A significant ($p < 0.10$) decreasing trend of -0.102 m s^{-1}/10 years is exhibited by the annual maximum gust speeds over the period 1928–2011, while a non-significant ($p > 0.10$) positive trend characterizes the entire period 1928–2020 of wind measurements. A turning point has been detected in the monthly maximum gust speed series in 2012, followed by a trend reversal. Distinctive differences in the gust trend pattern have been observed among the seasons, with increasing trend in summer, and winter gust speeds exhibiting decline in 1969–2011 and strengthening since 2012. Variations in the monthly maximum gust speeds appear closely related to changes in air temperature and latitudinal pressure gradients. Furthermore, the monthly maximum gust speeds show significant correlation with the main oceanic-atmospheric circulation patterns in the North Atlantic region. A synergistic effect among the phases of the dominant patterns of climate variability appears to explain the observed decline and recovery trends in winter gusts. Summer gust speeds show a positive correlation with the global land-ocean temperature deviations from the corresponding 1951–1980 base period mean.

1. Introduction

Near-surface wind is a primary driver in determining the exchanges of heat, water vapor and momentum between the Earth's surface and the atmosphere. Accurate estimation of wind speed is therefore of utmost importance not only in a wide range of scientific areas but also in engineering applications, due to the huge socio-economic consequences associated with the impact of adverse conditions (Munich Re, 2002; Spinoni et al., 2020; Insurance Journal website, https://www.insurancejournal.com/). Reliable estimates of extreme wind speeds and gusts are essential in determining design loads for buildings, infrastructure and transmission line systems (Aboshosha et al., 2016; Cook, 2007), in investigating the impact of wind storms on road, rail, water and air transport and related operations (Lam et al., 2017; Perry & Symons, 1994), in assessing the structural loading on wind turbines and changes in their output power (Anderson, 2020), and in estimating wind damage to trees and forests (Gardiner, 2021; Valta et al., 2019). Extreme winds are also the common atmospheric origin of extreme waves and storm surges (Masina et al., 2015; Vose et al., 2014), whose combined action leads to increased water levels at the coast and can cause significant erosion and flooding events in low-lying coastal areas. Furthermore, near-surface wind speed has relevant implications on the evaporation process (Stephens et al., 2018), dispersion of urban air pollutants (Yang et al., 2020), propagation of fire fronts (Hu, 2017), soil erosion (Zhang et al., 2019) and transport of dust particles (Menut, 2008).

Quantifying the spatial and temporal variability of wind is also extremely important, especially when small changes may have a substantial impact. In summer 2021 exceptionally low wind conditions across the UK severely affected the electricity cost and the renewable energy sector as a whole (Ambrose, 2021; Milne, 2021).

Examining an extensive data set of satellite records, statistically significant positive trends were highlighted by Young and Ribal (2019) in both mean and extreme (90th percentile) wind speeds over the period 1985–2018, with the strongest increases in the extreme conditions and in the Southern Ocean. Conversely, analyzing in situ anemometer measurements, various studies (reviewed by McVicar et al., 2012, Wu et al., 2018, and Zha

et al., 2021) documented a decrease in near-surface wind speed (termed "stilling" by Roderick et al., 2007) in the last 30–50 years over continental areas mostly across mid-latitudes of the Northern Hemisphere.

By using the sub-daily station based HadISD data set, Dunn et al. (2016) estimated that, globally (excluding Australia), terrestrial surface wind speeds declined at a rate of $-0.087\ m \cdot s^{-1}$/10 years during the period 1979–2015. On regional scale, the most pronounced decreasing trends were observed in Central Asia and North America, reaching respectively -0.151 and $-0.100\ m \cdot s^{-1}$/10 years. The weakest change over the same period, $-0.062\ m \cdot s^{-1}$/10 years, was estimated for Australia by using an updated version of the data set constructed by McVicar et al. (2008). A decreasing trend of $-0.087\ m \cdot s^{-1}$/10 years, corresponding to the intensity of the global phenomenon, was reported by Dunn et al. (2016) for Europe.

Decreasing trends of various magnitude have been found in Europe in a number of studies: mainly by analyzing 10 min mean wind speed data (Azorin-Molina et al., 2014; Laapas & Venäläinen, 2017; Minola et al., 2016; Pirazzoli et al., 2010) or hourly mean wind speeds (Früh, 2013; Shu & Jesson, 2021), and only to a lesser extent through maximum 3 s gusts (Azorin-Molina et al., 2016; Brázdil et al., 2017; Hewston & Dorling, 2011).

In particular, at the north-western edge of the European continent, facing the North-East Atlantic Ocean, a considerable long-term wind variability has been detected among different observation sites. By using wind measurements recorded between the 1950s and 2008, Pirazzoli et al. (2010) found annual average and extreme (99th percentile) wind speeds to decrease sharply at southwestern Iceland (Reykjavick), along the western coast of Ireland (Shannon and Valencia) and near the French Atlantic coast (Brest). Decreased wind speeds were also observed over Scotland by Früh (2013) in records long up to 43 years. However, increasing trends were identified by Pirazzoli et al. (2010) in the annual average wind speed of meteorological stations located between latitude 59°N (Kirkwall, off northern Scotland) and 62°N (Thorshavn, Faroe Islands) during the period mentioned above, and by Shu and Jesson (2021) in the South-East England between 1981 and 2018. It should also be noted that Shu and Jesson (2021) identified statistically significant long-term trends in annual mean wind speed in only 15 of the 38 UK stations analyzed. This might be in part due to the relatively short length of the data series examined.

A reversal in terrestrial stilling with a slight recovery of wind speed during the most recent decade has been documented for China (Yang et al., 2012), South Korea (Kim & Paik, 2015), Saudi Arabia (Azorin-Molina, Rehman, et al., 2018) and Sweden (Minola et al., 2022). Zeng et al. (2019) identified a significant turning point in the time series of regional-average mean annual wind speed that occurred earlier in Asia (2001) and Europe (2003) than in North America (2012), while also reported that the most significant increase in wind speed was observed after 2010 in all three regions.

The actual causes of the decline observed in the near-surface wind speed and of its recent recovery are largely uncertain. A number of possible causes has been hypothesized for the terrestrial wind stilling, whose contribution varies in importance across the different regions, including: (a) variations in the large-scale atmospheric circulation patterns (Azorin-Molina et al., 2016, 2021); (b) a poleward expansion of the Hadley cell under global warming, which induces a poleward shift of the North Atlantic jet and an eastward extension of the North Atlantic storm track into Europe (Li et al., 2018; Lu et al., 2007); (c) an increase of surface roughness due to forest growth, land use changes and urbanization (Vautard et al., 2010; Wu et al., 2017); (d) increased aerosol emissions and greenhouse gas concentrations (Bichet et al., 2012); (e) instrumental issues such as anemometer aging, which could lead to a gradual drift in historical wind speed series (Azorin-Molina, Asin, et al., 2018), and artificial variations in wind measurements caused by changes in the instrumentation and/or in the environmental conditions nearby the meteorological station (Suomi & Vihma, 2018).

As pointed out by Azorin-Molina et al. (2021), research studies analyzing long-term trend or multi-decade variability in wind gust records are still relatively limited compared to those dealing with wind speeds. This is mainly due to inhomogeneity problems, mostly related to changes in instrumentation, positioning and observational practice, which affect in particular the gust speed time series and often lead to not considering the early measurements or even to completely excluding gust data from the analyses.

The primary objectives of this study are: (a) to investigate the trend in the magnitude of the maximum gust speeds in one of the longest instrumental wind records in the UK, collected at St Mary's in the Isles of Scilly, and not included in most previous regional studies (Earl et al., 2013; Hewston & Dorling, 2011; Shu & Jesson, 2021; Watson et al., 2015); and (b) to evaluate the influence of climate variability on the observed maximum wind gusts. The results of the study contribute to a better understanding of the changes in the gust speeds at the

north-western edge of Europe and give new insights into the effects of global climate change. Furthermore, these results can provide insights for the assessment of the wind resource to optimize energy production as well as for the load analysis of structures and installations at the southernmost end of the UK (e.g., Khosroshahi et al., 2022).

2. Data

2.1. Site Details

Covering an area of about 6.5 Km^2, St Mary's is the largest of the Isles of Scilly, an archipelago of around 140 low-lying granite islands, comprising five main inhabited islands, several uninhabited islands and islets and numerous smaller rocky outcrops, located approximately 45 km south-west of Land's End, the most westerly headland of Cornwall (Figure 1).

The Isles of Scilly are fully exposed to the Atlantic Ocean and to prevailing southwesterly winds. In general, the strongest winds and gusts occur during the period from September to March and are associated with the eastward passage of deep depressions across or close to the British Isles. For their low-lying character the Isles of Scilly are among the most vulnerable islands in Europe (Petzold, 2017), directly affected by the impact of sea level rise and storm events causing coastal erosion and inundation.

The entire island group is a highly protected area for its unique natural environment and landscape of historical value (Council of the Isles of Scilly, 2021).

Since the late nineteenth century, with the development of the flower farming industry, the island landscape that had remained largely treeless until then began to be characterized by tall evergreen shrubs planted widely as windbreaks along the edges of small fields to protect bulbs from strong winds and salt-spray (Hooley, 2016). These field boundaries, protected under the 1997 Hedgerows Regulations (Kirkham et al., 2011), are a distinctive feature of the Scilly's farmed landscape.

The Isles of Scilly have a very small resident population (2,203 residents at 2011 census, https://statistics.ukdataservice.ac.uk/). The majority of the population live on St Mary's (1,723 residents) and is concentrated in Hugh Town, the administrative center for the islands. The village of Hugh Town is located on the low and narrow sandy isthmus which connects the fortified headland of Garrison to the south-west with Buzza Hill and the bulk of St Mary's to the east. The second highest concentration of population is at Old Town, the ancient medieval center of the islands, located on the southern side of St Mary's. Approximately 300 m east of Old Town there is St Mary's Airport, inaugurated on 15 September 1937. The rest of St Mary's is sparsely populated and rural in character, with scattered hamlets and farms (Figure 1).

By comparing the land use map created from the 1930s Land Utilisation Survey of Great Britain (freely accessible through the website https://www.visionofbritain.org.uk/maps/), with the 25 m raster version of the 2007 and 2015 Land Cover Maps (https://data.gov.uk/), and the Interactive Policy Map of the Council of the Isles of Scilly (2021), it can be seen that development on St Mary's has been mainly concentrated through time around major settlements.

2.2. Wind and Gust Measurements

Broomfield (1982) reported that a telegraphic reporting station was established on St Mary's on 1 January 1871, with observations initially taken twice a day (at 8:00 and 14:00). According to the Monthly Weather Reports of the UK Meteorological Office (Met Office, 2021b), a Robinson anemometer with 5 inch cups was installed at Garrison in 1879 and remained in operation until November 1927. In 1895 St Mary's was selected along with the Welsh Holyhead, facing the Irish Sea, as observation site to test the mode of wind measurement developed by William Henry Dines. Thus, between 20 and 27 August of the same year, a pressure tube anemometer was erected with the vane mounted on a stayed mast at 10 m above ground, alongside the Robinson anemometer, to allow the comparison of the measurements of the two instruments (Meteorological Council, 1896).

In November 1926 a Dines anemometer was erected at the Telegraph station, on the top of the coast guard lookout tower, with the vane placed at a height of 20 m above the ground and an estimated "effective height" of 17 m; since February 1928 this instrument was adopted as standard (Met Office, 2021b). This station (WMO 03804, Met Office Integrated Data Archive System [MIDAS] station identifier 1385), located on the north-west side

10.1029/2022EA002380

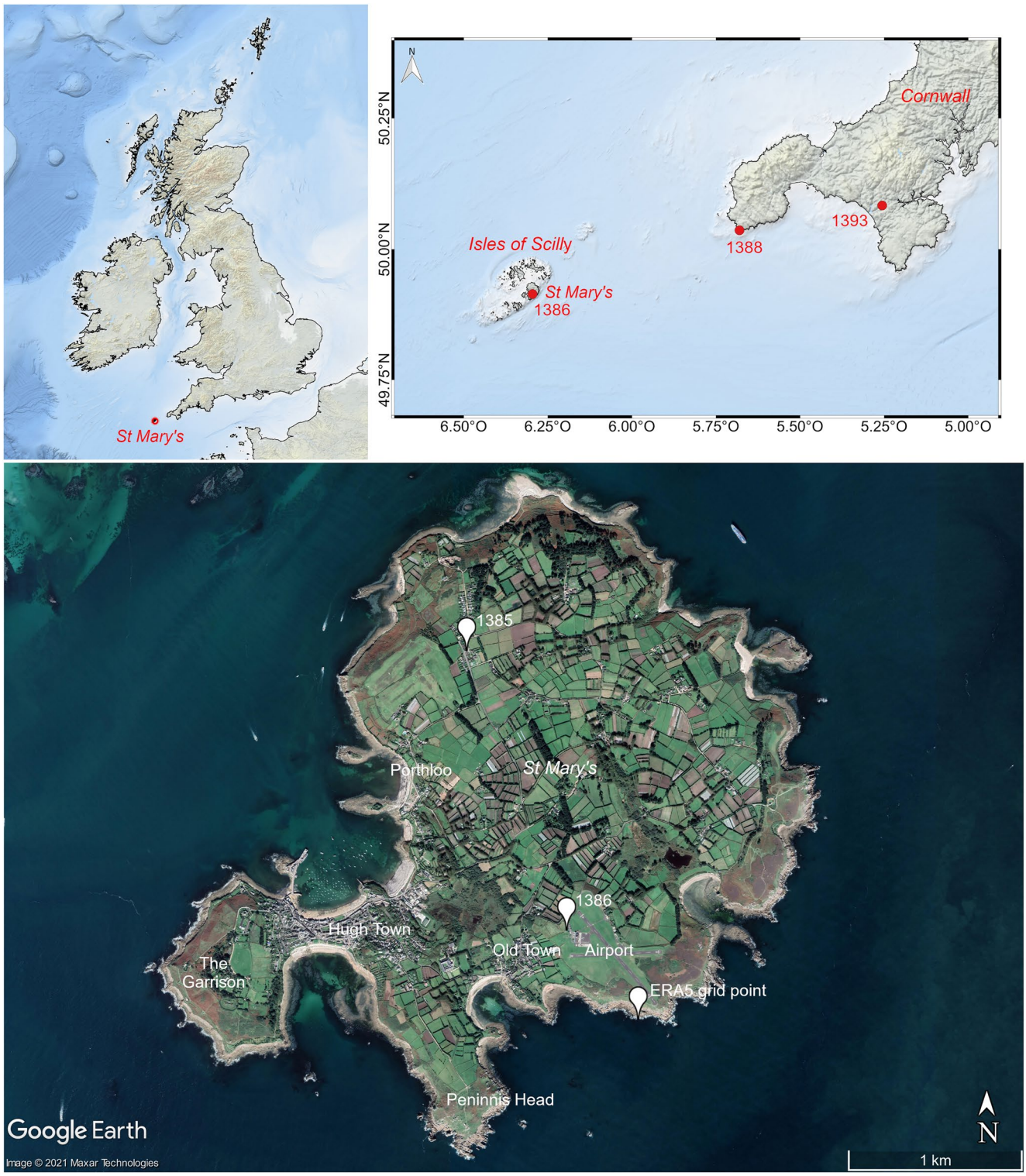

Figure 1. Map of the study site showing the location of the meteorological stations through their Met Office Integrated Data Archive System identifier and the ERA5 grid point considered in the analysis.

of the island on its highest point, approximately 50 m above m.s.l. (Figure 1), provided a continuous record, with only occasional outages, until December 1981, when the coast guard complement at St Mary's was reduced and therefore the possibility of obtaining regular meteorological observations was lost (Broomfield, 1982).

As reported by Met Office (2019), an automatic weather station, belonging to the Met Office network of synoptic stations, has been operational since 1 January 1979 at St Mary's Airport, on the southern coast of the island at about 30 m above m.s.l. (WMO 03803, MIDAS station identifier 1386) (Figure 1).

For the analysis presented here, wind data were extracted from the MIDAS Land and Marine Surface Stations Data (1853-current), stored in the Centre for Environmental Data Analysis (CEDA) Archive (Met Office, 2012). These data comprise hourly mean wind speeds and directions and maximum gust speed in an hour, along with its direction and occurrence time. In particular, the wind and gust data used in the analysis refer to measurements performed over a whole hour. The data made available through the CEDA Archive include the wind records collected during the interval 1 January 1969 to 26 December 1981 at the historical Scilly/St Mary's coast guard station (MIDAS identifier 1385) and the measurements of the period 21 October 1991 to 31 December 2020 at the Scilly/St Mary's Airport station (MIDAS identifier 1386).

The actual geographical location of each of the two weather stations, shown in Figure 1, has been determined through the analysis of the metadata stored in the CEDA Archive, jointly with the examination of the historical images available in Google Earth. Unfortunately, characteristics and changes over time in instrumentation, exposure and observing practice, which may have a significant impact on the wind measurements, are not documented in the freely available observational metadata accompanying the MIDAS data set. Accounting for the standard height of the UK network of surface stations, that is, 10 m above ground level (Sunter, 2021), the same height has been assumed for the cup anemometer at St Mary's Airport by visual inspection of photos embedded in Google Maps, since specific information about the height of the anemometer is not readily available.

Even though the UK Met Office began to gradually replace the Dines pressure tube anemometers with electrical cup generator anemometers during the 1950s, a Dines anemometer was still in use at the St Mary's coast guard station until at least December 1978 (Halliday, 1984). Prior to the advent of digital recording, the gust speeds were recorded on an anemograph, from which the values were manually read (Sloan & Clark, 2012). Since the 1970s automated observing systems were introduced by the Met Office to replace manned stations: initially the Digital Anemograph Logging Equipment (DALE), then the Synoptic Automatic Weather Station (SAWS), the Enhanced SAWS (ESAWS), the Semi-Automatic Meteorological Observing System (SAMOS) and, more recently, the Meteorological Monitoring System (MMS). Since the introduction of SAMOS in the 1980s, the wind speed was sampled every ¼ s, from which rolling 3 s mean values were calculated and the maximum used as the gust speed, according to the World Meteorological Organization (WMO) recommendation (Sloan & Clark, 2012).

The highest gust speeds for the years from 1928 to 1968 published in the Monthly Weather Reports (Met Office, 2021b) were also considered to reconstruct the observed gust time series at St Mary's. Only speed and direction of the maximum hourly mean wind occurred in the same day of the highest gust speed are available in the Monthly Weather Reports within the table listing occasions of strong gales. The direction of maximum gust has been reported in the aforementioned reports starting from 1960 onwards.

For comparative purposes, wind data were also retrieved from the MIDAS data set for the nearest meteorological stations of mainland England, Gwennap Head (WMO 03806, MIDAS identifier 1388) and Culdrose (WMO 03809, MIDAS identifier 1393), at about 66 and 76 m above m.s.l. (Figure 1). The data available in digital format for the Gwennap Head and Culdrose stations cover the periods 1971–1992 and 1977–2020 respectively.

2.3. Wind Gust From ERA5 Reanalysis

ERA5 reanalysis data have been analyzed to evaluate their performance in representing the observed values of maximum wind gust and their long-term variation at the study site. Gust speeds have been extracted from the ERA5 outputs at the grid point closest to the St Mary's Airport weather station (Figure 1), through the Copernicus Climate Change Service (http://climate.copernicus.eu/) implemented by the European Centre for Medium-Range Weather Forecasts (ECMWF). ERA5 is the fifth generation ECMWF reanalysis of the global climate, produced using a hybrid incremental 4-dimensional variational data assimilation scheme in the cycle Cy41r2 of the Integrated Forecasting System (IFS), which was operational in 2016 (Hersbach et al., 2020). ERA5 reanalysis products are available at a horizontal resolution of 31 km on 137 levels in the vertical up to 80 km and with a temporal resolution of 1 hr spanning 1950 onwards.

Conventional in situ and satellite measurements are used as input in ERA5. However, it is noteworthy that the 10 m wind observations over land are blacklisted by ECMWF and excluded from the data assimilation system.

The calculation of wind gust in ERA5 reanalysis is designed to ensure that the model output is compatible with the observing practice of the WMO for wind extremes (ECMWF, 2016). In particular, the wind gust is calculated at each simulation time step as sum of three terms, representing respectively the instantaneous 10 m wind speed, the turbulent gustiness and the convective contribution, and its maximum value since the last post-processing (in the last hour) is written in the output file.

2.4. Air Temperature and Mean Sea Level Pressure Data

Hourly data of air temperature and msl pressure recorded by the meteorological stations of Scilly/St Mary's (MIDAS identifier 1385) and Scilly/St Mary's Airport (MIDAS identifier 1386) have been derived through the CEDA Archive, where measurements are available for the periods 1958–1981 and 1985–2020 respectively (Met Office, 2021a).

Monthly values of mean, minimum and maximum air temperature and sea level pressure extracted from the HadUK-Grid data set (Hollis et al., 2019; Met Office et al., 2021) at the grid point closest to the St Mary's Airport station have also been used in the analysis. The time series of air temperature and pressure obtained by this data set cover the periods 1884–2020 and 1961–2020 respectively and are based on the records derived from the network of UK land meteorological stations interpolated onto a 1×1 km grid.

Mean air temperature and msl pressure recorded by the meteorological stations of Valentia Observatory (Ireland) and Santa Cruz de Tenerife (Canary Islands, Spain), at latitudes of 51.94°N and 28.46°N respectively, have been analyzed to investigate the effect of air temperature and pressure gradient variations on the observed gust speed changes. Daily values of mean air temperature and msl pressure for these two stations have been derived through the websites of the European Climate Assessment & Data set project (https://www.ecad.eu/; Klein Tank et al., 2002) and Met Éireann, The Irish Meteorological Service (https://www.met.ie/climate/available-data/historical-data). The Valentia and Santa Cruz time series cover the periods 1940–2020 and 1933–2020 respectively.

2.5. Large-Scale Climate Indices

Following previous studies which investigated the influence of large-scale oceanic-atmospheric circulation patterns on wind speed variability (Zeng et al., 2019; Zhou et al., 2021), a set of 19 climate indices has been considered in the present analysis. The climate indices are listed in Table 1 along with a brief description and source of the data. These climate indices have been selected because they characterize major aspects of oceanic-atmospheric variability. Indeed, the group includes indices representing large-scale atmospheric circulation, sea surface temperature (SST) anomalies in the Atlantic Ocean, El Niño Southern Oscillation (ENSO) phenomenon and combined land-surface air and sea-surface water temperature anomalies. The indices are provided as monthly time series except for the Western Europe Pressure Anomaly (WEPA), which is given as a winter averaged (December to March, DJFM) time series. The most influential climate indices have been determined through a correlation analysis with the homogenized monthly maximum gust speeds.

3. Methods

3.1. Data Quality Control

The data in the climate database MIDAS have undergone a series of systematic quality control checks by the Met Office to ensure consistency of the observations (Sunter, 2021). Therefore, only the records flagged as quality checked by the Met Office were used in this study. Duplicate records were removed, retaining only the most recent version of the entry. The data set was then subjected to careful visual inspection and further quality checks to guarantee its accuracy. Some erroneous historical data were identified through a coherency cross-check among associated parameters within each hourly record and removed as violating logical or physical relationships. Through a temporal consistency check, some doubtful repeated values were further identified and eliminated. By examining the relationship between the gust factor—defined as the ratio of the peak wind gust to the

Table 1
List of the Climate Indices Used in the Study and Source of Data[a]

Climate index	Classification	Period	Description	Source
CRU North Atlantic Oscillation (CRU NAO)	Atm. circ.	1821–2020	Normalized SLP difference between Gibraltar and SW Iceland	CRU (2021a)
CPC North Atlantic Oscillation (CPC NAO)	Atm. circ.	1950–2020	From RPCA applied to 500 hPa height anomalies over 20°N–90°N	NOAA CPC (2021c)
Instrumental East Atlantic Pattern (SLP Val)	Atm. circ.	1866–2016	Standardized SLP anomalies from Valentia Observatory, Ireland	Comas-Bru and Hernández (2018a)
CPC East Atlantic Pattern (CPC EA)	Atm. circ.	1950–2020	From RPCA applied to 500 hPa height anomalies over 20°N–90°N	NOAA CPC (2021a)
Instrumental Scandinavian Pattern (SLP Ber)	Atm. circ.	1901–2017	Standardized SLP anomalies from Bergen Florida, Norway	Comas-Bru and Hernández (2018a)
CPC Scandinavian Pattern (CPC SCA)	Atm. circ.	1950–2020	From RPCA applied to 500 hPa height anomalies over 20°N–90°N	NOAA CPC (2021d)
East Atlantic/Western Russia Pattern (EA/WR)	Atm. circ.	1950–2020	From RPCA applied to 500 hPa height anomalies over 20°N–90°N	NOAA CPC (2021b)
Western Europe Pressure Anomaly (WEPA)	Atm. circ.	1943–2018	Normalized SLP gradient between Valentia and Santa Cruz de Tenerife	Scott et al. (2020)
Tropical/Northern Hemisphere Pattern (TNH)	Atm. circ.	1950–2020	From RPCA applied to 500 hPa height anomalies over 20°N–90°N	NOAA CPC (2021e)
Southern Oscillation Index (SOI)	Atm. circ.	1866–2020	Normalized SLP difference between Tahiti and Darwin	CRU (2021b)
Atlantic Meridional Mode-SST (AMM-SST)	SST, Atlantic	1948–2020	From MCA to SST over 21°S–32°N, 74°W–15°E	NOAA PSL (2021)
Atlantic Meridional Mode-wind (AMM-wind)	Wind, Atlantic	1948–2020	From MCA to 10 m wind field over 21°S–32°N, 74°W–15°E	NOAA PSL (2021)
ENSO Longitude Index (ELI)	SST, ENSO	1854–5/2020	Average longitude of tropical Pacific deep convection	Williams and Patricola (2020)
Niño 3	SST, ENSO	1870–2020	Area averaged SST anomalies over 5°N–5°S, 150°W–90°W	GCOS-WGSP (2021b)
Niño 3.4	SST, ENSO	1870–2020	Area averaged SST anomalies over 5°N–5°S, 170°W–120°W	GCOS-WGSP (2021c)
Niño 4	SST, ENSO	1870–2020	Area averaged SST anomalies over 5°N–5°S, 160°E−150°W	GCOS-WGSP (2021d)
Niño 1+2	SST, ENSO	1870–2020	Area averaged SST anomalies over 0°N–10°S, 90°W–80°W	GCOS-WGSP (2021a)
Global Land-Ocean Temperature Index (GLOTI)	Temperature	1880–2020	Global land-ocean temperature anomalies relative to the 1951–1980 base period	GISTEMP Team (2021)
Northern Hemisphere Land-Ocean Temperature Index (NHLOTI)	Temperature	1880–2020	Northern Hemisphere land-ocean temperature anomalies relative to the 1951–1980 base period	GISTEMP Team (2021)

[a]SLP, sea level pressure; SST, sea surface temperature; Atm. circ., atmospheric circulation; ENSO, El Niño Southern Oscillation; RPCA, rotated principal component analysis; MCA, maximum covariance analysis.

mean wind speed—and the hourly mean wind speed, some outliers associated with anomalously high gust values were detected, which were deemed as spurious data and therefore removed.

The concurrent wind measurements recorded at Culdrose, the nearest available neighbor station, were also examined to evaluate the inter-station consistency and ensure spatial coherency.

The wind and gust speed measurements, recorded in integer knots, were converted to meters per second ($m \cdot s^{-1}$).

3.2. Data Homogenization

Changes in the instrumentation employed, observing practice, measurement height and observing site give rise to significant discontinuities in the gust speed time series. A discontinuity is evident between the gust speeds recorded by the Dines anemometer at the historical coast guard station and those measured at St Mary's Airport after 21 October 1991. Similar discontinuities were also observed by Chen (1975), Logue (1989), Cechet and Sanabria (2015), and Bakker and Viljoen (2019), by analyzing gust speed data from stations in Hong Kong, Ireland, Australia and South Africa respectively, where the Dines anemometer was the main wind measuring instrument until being replaced by automatic weather stations with cup anemometers between the 1980s and 1990s.

By comparing the wind speeds recorded simultaneously in 1984 at Galway (Ireland) by a Dines pressure tube anemometer and a Munro Mark 2 cup anemometer, Logue (1986) noted a generally good agreement between the hourly mean wind speeds measured by the two instruments and maximum gust speeds recorded by the Dines anemometer on average 6%–7% higher than those from the cup anemometer. The results obtained by Logue (1986) for the maximum gust speeds are in agreement with findings of Cechet and Sanabria (2015), who analyzed concurrent gust speed measurements from Dines anemometers and Synchrotac cup anemometers at seven stations in northern Australia. The latter authors observed that at gust speeds of about 45 $m{\cdot}s^{-1}$ the Dines anemometer tended to report gusts that were about 5%–10% higher than those obtained from the cup anemometer, increasing to about 12%–17% for gust speeds around 60 $m{\cdot}s^{-1}$.

To tackle the discontinuity in the gust records, the approach outlined by Turner et al. (2019) has been followed in the homogenization of St Mary's data. By using the measured hourly mean wind speeds ($\overline{U}$) and the maximum gust speeds ($\hat{U}$) over the 1 hr period, gust factors can be calculated by directional sectors for each of the two St Mary's observation sites, providing useful information on the turbulence intensity (I_u) and hence on the effective roughness length (z_0). This latter can be used to derive appropriate directional correction factors for adjusting the measured gust speeds to the standard conditions of 10 m height in flat open country terrain characterized by a roughness length z_0 of 0.03 m. This value, equivalent to typical UK open countryside, was historically assigned to category II terrain in the British Standards for the design wind loading (Cook, 1985, 2007).

In deriving the correction factors, hourly mean wind speeds lower than or equal to 5.5 $m{\cdot}s^{-1}$ have been excluded from the analysis to ensure nearly neutral conditions, according to the atmospheric stability classification proposed by Pasquill (1961). In the atmospheric surface layer under nearly neutral conditions, the variation in the mean wind speed with height can be described by the logarithmic law

$$U(z) = \frac{u_*}{k} \ln\left(\frac{z}{z_0}\right) \tag{1}$$

where k is the von Kármán constant (~0.40), u_* is the friction velocity, z is the height above the ground and z_0 is the surface roughness length.

Assuming the hourly mean wind speeds measured by the Dines anemometer in good agreement with those recorded by the cup anemometer, the gust speeds of the period 1969–1981 have been corrected using factors derived by Miller et al. (2013, their Table 2), which take into account the response characteristics of the Dines anemometer compared with those of a cup anemometer and the effect of adopting the WMO recommended 3 s gust definition. As outlined by Miller et al. (2013), the 3 s moving average applied to the cup anemometer output signal has the effect to truncate the high-frequency end of the wind spectrum, therefore leading to significantly lower peak gust values compared to those provided directly by the anemometer output.

For each of the two St Mary's stations, the available wind data have been divided into 16 cardinal directional sectors. The $\hat{U}$ and $\overline{U}$ values have been used to calculate the gust factor GF, which is the ratio of the maximum gust speed within a specified period to the mean wind speed:

$$\mathrm{GF}(T, t, z, z_0) = \frac{\hat{U}(t, z, z_0)}{\overline{U}(T, z, z_0)} \tag{2}$$

where T is the sample time, equal to 3,600 s in the case under consideration, and t is the gust duration, equal to 3 s. Sudden gust fronts resulting in high gust factors (GF > 2.5), mainly due to transient conditions, have been excluded from the analysis. The remaining GF values obtained from the same instrument in the same directional sector have been averaged to determine the expected mean GF value.

The expected mean gust factor can be obtained from Equation 3 (e.g., Holmes, 2015):

$$\mathrm{GF} = 1 + g\frac{\sigma_u}{\overline{U}} = 1 + g \cdot I_u \tag{3}$$

where g is the expected peak factor, defined as the ratio of the maximum wind speed fluctuation to the standard deviation of the fluctuating component of wind (σ_u), and depends on the averaging period T, gust duration t and measurement height z. I_u is the longitudinal turbulence intensity, defined as the ratio of the standard deviation of wind speed fluctuations to the mean wind speed.

The empirical relationship proposed by Cook (1985) for the gust factor

$$\mathrm{GF}(3600, t) = 1 + 0.42 \cdot I_u \cdot \ln(3600/t) \tag{4}$$

which assumes hourly wind records with arbitrary gust duration of t seconds, has been applied with $t = 3$ s to estimate the turbulence intensity I_u.

Assuming for σ_u/u_* a typical value of 2.5 for homogeneous flat terrain, from Equation 1 the turbulence intensity is given by

$$I_u = 1/\ln(z/z_0) \tag{5}$$

and the directional effective roughness length z_0 can be therefore calculated as follows:

$$z_0 = z \cdot \exp(-1/I_u)\,. \tag{6}$$

Based on each measured mean wind speed $\overline{U}$, measurement height z above the ground and estimated surface roughness z_0, the friction velocity u_* has been calculated by the logarithmic-law velocity profile (Equation 1), and the corresponding gradient wind speed U_g has been estimated through the relationship given by Irwin (2006):

$$\frac{U_g}{u_*} = \frac{1}{k}\left[\ln\left(\frac{u_*}{f \cdot z_0}\right) + 1\right] \tag{7}$$

where f is the Coriolis parameter defined by $f = 2 \cdot \omega \cdot \sin\varphi$, in which ω is the angular velocity of the Earth and φ the latitude of the weather station.

Following Turner et al. (2019), Equation 7 has been used to convert u_* to its equivalent value in the standard conditions, that is, over $z_0 = 0.03$ m, being the gradient wind speed relatively insensitive to the surface roughness. Then, the estimated standard u_* has been substituted into Equation 1, along with $z_0 = 0.03$ m and $z = 10$ m, to determine the standard hourly mean wind speed. The standard hourly mean wind speed has been then multiplied by the gust factor computed from Equation 4, to calculate the standard gust speed (e.g., Masters et al., 2010). Correction factors for $\hat{U}$ have been finally estimated by dividing the standard gust speed by the measured $\hat{U}$ (corrected when necessary for the anemometer response and gust duration), and averaging the resulting values over each directional sector.

The directional $\hat{U}$ correction factors, estimated for each of the two stations from the available GF values of the periods 1969–1981 and 1991–2020, have been subsequently applied to convert the gust speeds to the equivalent values in the standard conditions.

In order to evaluate the effect of topography on gust speed, the DTM LiDAR data collected in 2020 at 1 m spatial resolution by the UK Environment Agency have been examined (https://environment.data.gov.uk/). At each observation site the average slope has been calculated for profiles extracted along the 16 directional axes from the anemometer location up to a distance of 10 times the elevation of the station site. Considering the Dines anemometer location, the largest values of mean absolute slope have been obtained for the WNW and NW profiles, 6.6° and 5.8° respectively, due to their intersection with a cliff at the edge of the island. The mean absolute slopes in

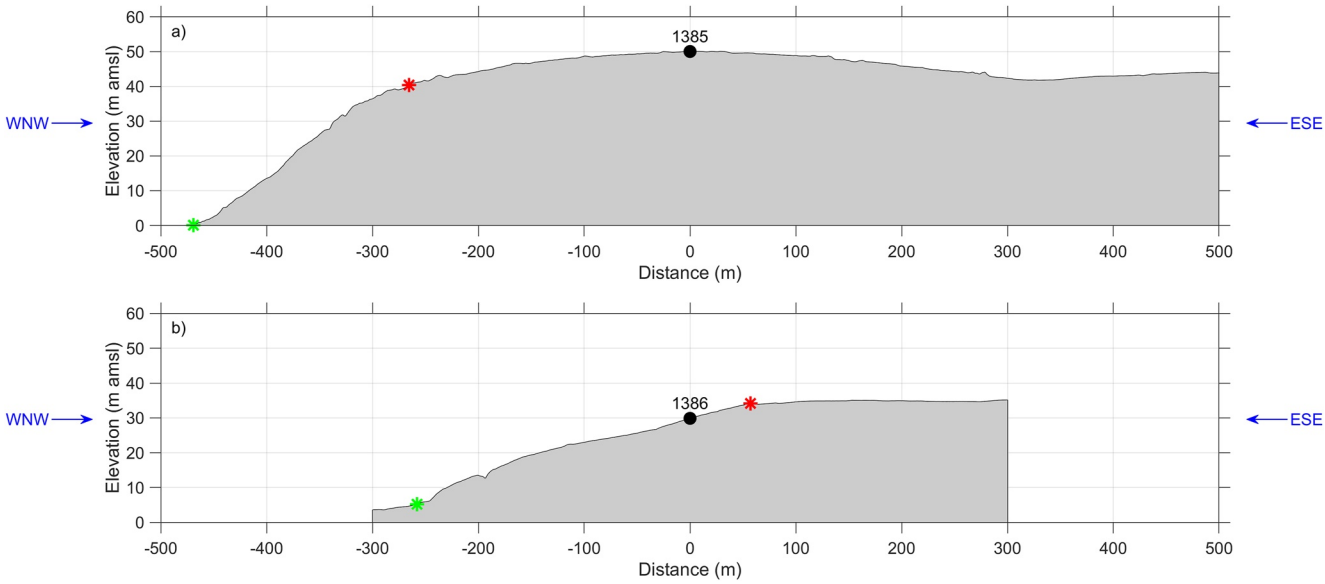

Figure 2. Ground elevation on WNW-ESE section at the sites of the (a) Dines and (b) cup anemometers from DTM LiDAR data. The black circle marks the anemometer location. The green and red asterisks identify the foot and peak of the escarpment considered in the application of the wind loadings standards.

the other directions are in the range of 1.6°–3.8°. Following the procedures outlined in the loadings standards BS EN 1991-1-4:2005 (BSI, 2011) and AS/NZS 1170.2:2011 (SA/SNZ, 2011) for determining the topographic wind speed multipliers, similar factors have been derived at a height of 10 m above ground level for the WNW wind direction, equal to 1.117 and 1.075 respectively (Figure 2a). For the cup anemometer at the airport, the largest values of mean absolute slope (4.2°–5.3°) have been found for the S to NNW profiles, with the maximum in WNW direction (as for the Dines anemometer), mainly due to the shallow elevations characterizing the Lower Moore wetland between Hugh Town and Old Town. According with the procedures described in BS EN 1991-1-4:2005 (BSI, 2011) and AS/NZS 1170.2:2011 (SA/SNZ, 2011), at the current position of the anemometer the topographic wind speed multipliers calculated at a height of 10 m above ground level for the WNW wind direction are 1.109 and 1.070 respectively (Figure 2b). Due to the low-lying character of St Mary's Island and its relatively gentle slopes, topographic effects were not removed in the data homogenization process.

Monthly maximum values have been identified from the homogenized gust speed time series. In particular, since January 1973, when hourly data resolution was adopted, maximum gust values have been identified for each month with at least 50% of potentially available observations. However, a further check has been carried out on the months of the 1973–2020 period with few observations to verify that extreme gust values had not been discarded. To ensure independence of the monthly maximum gust data, the selection has been performed considering events separated by at least 72 hr.

Severe wind gusts have been validated examining lists of extreme storm events and related documentation. By performing this cross-validation, the maximum gust speed (40.1 $m \cdot s^{-1}$) recorded by the St Mary's automatic weather station during the Burns' Day Storm of 25 January 1990 has been found within the work of Pike (1991). After adjustment through the corresponding correction factor, it has been added to the monthly maximum time series. During the Burns' Day Storm significantly higher gust values were recorded on the west coast of Cornwall: 47.8, 46.3, and 45.7 $m \cdot s^{-1}$ were measured at Gwennap Head, Land's End and Culdrose respectively (Blackall et al., 1990; Eden, 2008; McCallum, 1990).

Due to the high variability of wind gusts, the missing values and the data gap from January 1982 to October 1991 have not been filled using available measurements from neighboring stations, in order to preserve the natural variability of the observed gust data and avoid bias in the assessment of trend and dependence. Considering also the results obtained from the comparison between the anemometer gust speeds and ERA5 data, a reconstruction process through numerical modeling has not been attempted, as this might similarly introduce further inhomogeneities into the gust series seriously affecting subsequent analyses.

The penalized maximal F test has been applied to each of the two monthly maximum subseries relative to the periods 1969–1981 and 1991–2020, to detect any other potential changepoints or artificial shifts in the data. For this data homogeneity check, the "RHtestsV4" software package has been used without a reference series (Wang & Feng, 2013). Only one changepoint has been identified as statistically significant at the 5% level in May 2012. However, the time series of monthly maximum values has not been further corrected because the trend component estimated for the base series is preserved when applying the quantile matching adjustment algorithm implemented in "RHtestsV4" without a reference series, whereas a turning point has been documented in wind speed time series by several studies in the most recent decade (e.g., Zeng et al., 2019).

The spatio-temporal changes in population, cover and land use at St Mary's can be deemed to have had a negligible impact on the observed wind and gust speed variations. Hence, the historical time series of maximum gust speeds has been obtained by considering also the annual maximum values recorded by the coast guard station between 1928 and 1968, after their adjustment through the directional $\hat{U}$ correction factors previously calculated from the available Dines wind and gust measurements of the period 1969–1981.

3.3. Long-Term Trend Analysis

Sen slope estimator (Sen, 1968) has been used to evaluate data trend magnitude and sign. The Sen slope estimator is a non-parametric method widely applied to hydro-meteorological records for trend analysis, since it is insensitive to the presence of outliers and missing values (Gilbert, 1987) and thus more robust for skewed data. Various flavors of the non-parametric, rank based Mann-Kendall test have been adopted to evaluate the statistical significance of the trend and to account for the uncertainty related to the statistical testing method. Overall, these include:

i) The original Mann-Kendall trend test (Kendall, 1975; Mann, 1945), which does not consider serial correlation or seasonal effects (hereinafter referred to as MK1);
ii) The Mann-Kendall test with the trend-free pre-whitening approach proposed by Yue et al. (2002), where the effect of significant lag 1 serial correlation is removed from the time series before applying the trend test (MK2);
iii) The modified Mann-Kendall test using the variance correction approach proposed by Hamed and Rao (1998), in which the autocorrelation between the ranks of the detrended data is first evaluated and only significant lags of autocorrelation coefficients (at the 0.05 level) are used to correct the variance of the test statistic (MK3);
iv) The modified Mann-Kendall test using the variance correction approach proposed by Yue and Wang (2004), in which serial correlation coefficients for all lags are used in calculating the effective sample size (MK4);
v) The Mann-Kendall test taking into consideration the long-term persistence by estimating the Hurst coefficient of the series, according to the procedure suggested by Hamed (2008) (MK5).

Two different R packages have been used to perform these tests: "modifiedmk" (Patakamuri & O'Brien, 2021) for MK1, MK2, MK3, and MK4 tests and "HKprocess" (Tyralis, 2016) for MK5 test computation. Two significance levels, $p \leq 0.05$ and $p \leq 0.10$, have been applied for the trend tests, as proposed by McVicar et al. (2010) and Azorin-Molina et al. (2014, 2016) among others.

The long-term trend analysis, when performed on annual and seasonal series, has been carried out on the deseasonalized data, obtained by subtracting from each monthly observation the monthly mean, computed over the entire available data set, and dividing by the corresponding monthly standard deviation.

A trend analysis has also been applied on running windows of 30 and 15 years, to highlight different sub-periods of the mean air temperature and msl pressure time series dominated by positive or negative trends.

3.4. Correlation Analysis

The Kendall correlation coefficient (τ) (Kendall, 1970), which measures the strength of the monotonic association between two ranked variables, has been used to evaluate the relationship between the gust speed and the climatic variables mentioned above. The Kendall correlation coefficient has been selected as it is a rank-based statistics and, therefore, resistant to the effects of outliers.

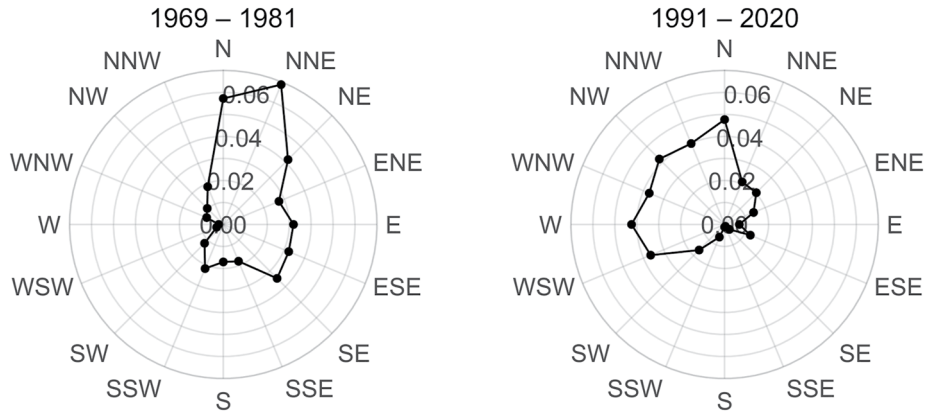

Figure 3. Effective roughness lengths (m) at the historical coast guard station (1969–1981) and St Mary's Airport (1991–2020).

4. Results and Discussion

4.1. Homogenized Gust Speeds

Gust and mean wind speeds recorded over 1 hr intervals have been used to estimate the effective roughness lengths (z_0) for the two anemometer locations: the historical coast guard station (1969–1981) and St Mary's Airport (1991–2020). The values of z_0 calculated for these two stations by using Equation 6 are shown in Figure 3. The estimated roughness lengths closely match the expected values for the terrain conditions around the stations.

The St Mary's historical coast guard station was located in the settlement of Telegraph. Therefore, buildings and trees within this settlement as well as those in McFarland's Down, immediately to the north, were primarily responsible for the highest roughness lengths (0.057 and 0.069 m) characterizing the N to NNE wind sectors. The lowest roughness lengths, 0.002–0.008 m, which are obtained for the directions between WSW and WNW, are typical values for unobstructed coastal areas directly exposed to sea waters. An effective roughness length of 0.01–0.03 m is estimated for the St Mary's rural landscape with fields and rows of windbreaks.

Table 2
Directional Gust Speed Correction Factors Calculated for the Anemometers at the Historical Coast Guard Station (1969–1981) and St Mary's Airport (1991–2020)

Wind direction	1969–1981	1991–2020
N	1.023	1.121
NNE	0.984	0.991
NE	0.971	0.988
ENE	0.960	0.976
E	0.952	0.953
ESE	0.960	0.965
SE	0.964	0.948
SSE	0.948	0.928
S	0.932	0.906
SSW	0.941	0.945
SW	0.923	0.973
WSW	0.892	0.999
W	0.883	1.021
WNW	0.903	1.018
NW	0.906	1.023
NNW	0.916	1.021

The automatic weather station at St Mary's Airport is located on the north-west side of the airfield. The low roughness lengths (~0.01–0.02 m) obtained for the directions between NNE and ESE are in agreement with characteristics values for runways and airport areas. The lowest roughness lengths (0.001–0.006 m) are encountered for the directions ranging from SE to SSW, and are typical values for coastal areas with no obstacles. The highest roughness lengths (from 0.036 to 0.048 m) are mainly determined by the presence of the centers of Old Town to southwest and Hugh Town to the west, and by a farm with cultivated fields bordered by vegetated windbreaks immediately to the north (Figure 1).

The directional $\hat{U}$ correction factors calculated for the two stations using the homogenization procedure described in Section 3.2 are shown in Table 2. The Dines gust speed measurements (1969–1981) have been first converted to the equivalent 3 s moving average gusts using the factors derived by Miller et al. (2013), and then corrected for the measurement height (i.e., from 17 to 10 m) and terrain roughness (i.e., from the calculated z_0 to the standard value of 0.03 m) by applying the factors of Table 2 (column 2). The 1991–2020 gust speed records have been adjusted solely for the effect of terrain roughness through the factors of Table 2 (column 3).

From the analysis of the correction factor values in Table 2, emerges that errors up to around 12% would be introduced in the subsequent analyses by

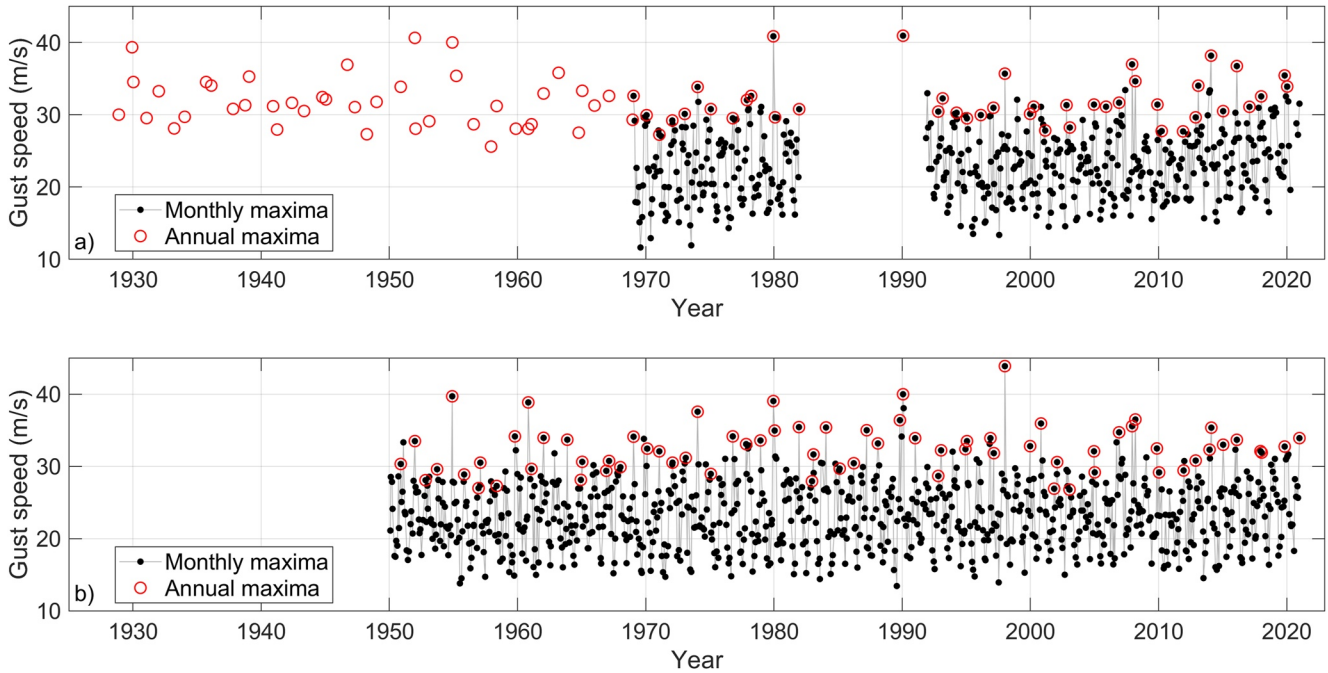

Figure 4. Annual and monthly maximum gust speed time series derived from (a) the homogenized measurements and (b) ERA5 reanalysis data.

not adjusting the measured gust speeds for differences in site exposure conditions. This result is in agreement with previous studies showing that direct use of gust speed measurements without homogenization and correction for terrain effects can introduce errors on the order of 10%–40% (Masters et al., 2010; Turner et al., 2019). This stresses the importance of eliminating all artificial shifts and terrain effects to ensure that the resulting time series reflects the real climatology of the area under study.

The homogenized annual and monthly maximum gust speed time series are shown in Figure 4a and analyzed in detail in the following Section 4.2. A comparison is also presented with the annual and monthly maximum gust speeds derived from the ERA5 reanalysis data (Figure 4b), that is discussed in Section 4.4.

4.2. Trends in Maximum Wind Gusts

Table 3 summarizes the long-term trends in maximum gust speeds. The results presented in Table 3 show that the magnitude and sign of gust speed trend, as well as its statistical significance, are strongly dependent on the starting date, observation length, time scale and statistical approach considered.

The analysis highlights that the homogenized annual maximum gust speeds decreased significantly ($p = 0.08$ for MK3 and $p = 0.02$ for MK4) at St Mary's at a rate of -0.102 m·s^{-1}/10 years during the period 1928–2011. By extending the analysis to the entire period 1928–2020, a non-significant trend of 0.055 m·s^{-1}/10 years ($p > 0.10$) is found. As indicated in Section 3.2, a statistically significant ($p < 0.05$) turning point has been identified at the beginning of 2012, followed by a marked reversal in trend and recovery of gust speed during the last 9 years.

Considering the monthly maximum gust speeds, a statistically non-significant positive trend ($p > 0.10$) is observed annually over the period 1969–2011, while a significant increasing trend is estimated during 1969–2020 (0.16 m·s^{-1}/10 years, $p < 0.05$).

The results indicate that, due to the high interannual variability, only the longer time series allows to detect a statistically significant decreasing trend on annual scale. The magnitude of the decreasing trend estimated from the annual maximum gust speeds appears in line with results of previous studies on the Northern Hemisphere mid-latitude wind stilling, generally on the order of -0.10 m·s^{-1}/10 years (e.g., Wu et al., 2018), and also the observed recovery since 2012 is consistent with the increase in near-surface wind speed outlined by Zeng et al. (2019) at global scale after 2010.

Table 3
Sen Slope Values Estimated for the Annual and Monthly Maximum Gust Speeds From the Homogenized and ERA5 Reanalysis Data

			Homogenized gust speeds				ERA5 reanalysis gust speeds				
			Sen slope ($m \cdot s^{-1}$/10 years)				Sen slope ($m \cdot s^{-1}$/10 years)				
	Series	Period	MK1	MK2	MK3	MK4	MK1	MK2	MK3	MK4	MK5
Annual max		1928–2020	0.055	0.051	0.055	0.055					
		1928–2011	−0.102	−0.141	**−0.102**	**−0.102***					
		1950–2020	0.366	**0.418**	**0.366**	**0.366***	0.296	0.289	**0.296**	**0.296***	0.296
		1950–2011	0.048	0.166	0.048	0.048	0.366	0.345	0.366	**0.366***	0.366
Monthly max	Annual	1969–2020	**0.157***	**0.161***	**0.157***	**0.157***	**0.060***	**0.062***	**0.060***	**0.060***	**0.060***
		1969–2011	0.024	0.031	0.024	0.024	0.022	0.026	0.022	**0.022**	0.022
	DJF	1969–2020	0.047	0.067	0.047	0.047	−0.034	−0.024	−0.034	−0.034	−0.034
		1969–2011	**−0.212***	**−0.193***	**−0.212***	**−0.212***	**−0.152***	**−0.142***	**−0.152***	**−0.152***	**−0.152***
	MAM	1969–2020	**0.150**	**0.134**	**0.150**	**0.150***	0.066	0.055	0.066	**0.066***	0.066
		1969–2011	0.150	0.130	0.150	**0.150***	0.102	0.090	0.102	**0.102***	0.102
	JJA	1969–2020	**0.282***	**0.294***	**0.282***	**0.282***	**0.147***	**0.152***	**0.147***	**0.147***	**0.147***
		1969–2011	**0.177**	**0.199***	**0.177**	**0.177***	0.108	0.119	**0.108**	**0.108***	0.108
	SON	1969–2020	**0.189***	**0.177***	**0.189***	**0.189***	0.063	0.054	0.063	**0.063***	0.063
		1969–2011	0.042	0.012	0.042	0.042	0.045	0.029	0.045	**0.045**	0.045
	January	1969–2020	−0.530	−0.450	−0.530	**−0.530**	−0.496	−0.466	−0.496	**−0.496***	−0.496
	February	1969–2020	0.620	0.779	0.620	**0.620**	−0.024	−0.016	−0.024	−0.024	−0.024
	March	1969–2020	0.506	0.359	0.506	**0.506***	−0.082	−0.090	−0.082	−0.082	−0.082
	April	1969–2020	0.108	0.272	0.108	0.108	0.044	0.071	0.044	0.044	0.044
	May	1969–2020	0.936	0.974	**0.936***	**0.936***	**0.551**	0.497	**0.551**	**0.551***	**0.551**
	June	1969–2020	**0.736**	**0.806**	**0.736**	**0.736***	0.429	**0.514**	**0.429***	**0.429***	0.429
	July	1969–2020	**1.093***	**1.075***	**1.093***	**1.093***	**0.543***	**0.594***	**0.543***	**0.543***	**0.543***
	August	1969–2020	**0.813**	0.484	**0.813**	**0.813***	0.236	0.104	0.236	0.236	0.236
	September	1969–2020	−0.035	−0.213	−0.035	−0.035	−0.053	−0.147	−0.053	−0.053	−0.053
	October	1969–2020	0.678	0.524	**0.678**	**0.678***	0.012	−0.161	0.012	0.012	0.012
	November	1969–2020	**1.209***	**1.359***	**1.209***	**1.209***	**0.533**	**0.616***	**0.533***	**0.533***	**0.533**
	December	1969–2020	0.473	0.487	0.473	**0.473**	0.166	0.118	0.166	0.166	0.166

Note. Statistically significant trends at $p \leq 0.10$ level are indicated in bold and at $p \leq 0.05$ level in bold and with an asterisk.

Differences in magnitude, sign and significance emerge when examining seasonal and monthly gust trends over the period 1969–2020 (Table 3). Seasonally, the strongest significant increasing trend ($p < 0.05$) is found in summer, while winter exhibits the weakest and non-significant positive trend ($p > 0.10$). At the monthly scale, the strongest increasing trends are found in November and July ($p < 0.05$), while decreasing trends are encountered in January ($p < 0.10$ for MK4 and $p > 0.10$ for MK1, MK2, and MK3) and September ($p > 0.10$).

From the analysis of the trend results in Table 3, the accuracy of the two modified MK tests MK3 and MK4 considering variance correction approaches is found to be superior to that of the original MK test (MK1) and MK test with trend-free pre-whitening (MK2). An increase in significant trend detection is found when the full autocorrelation structure exhibited by the time series is considered. Negligible differences from the original MK1 test are observed when only the lag 1 autocorrelation (MK2) is taken into account.

The break in the stilling detected in the homogenized gust speeds is highlighted in Figure 5a by comparing the trends estimated separately for the three periods 1969–1981, 1992–2011, and 1992–2020. A comparison is also presented with the seasonal and monthly trends derived for the same three periods from the ERA5 reanalysis data (Figure 5b), that is discussed in Section 4.4. As a 9 year period is too short to derive accurate trend estimates, the

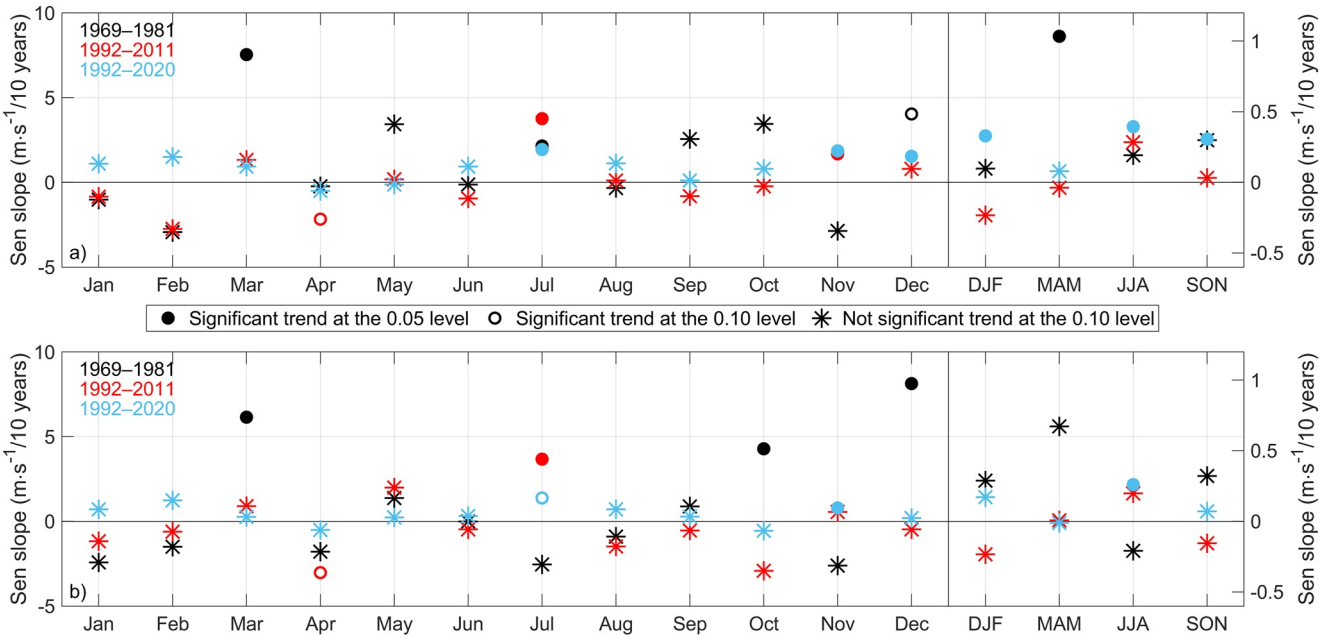

Figure 5. Seasonal and monthly trends of the monthly maximum gust speeds over the periods 1969–1981, 1992–2011, and 1992–2020 from (a) the homogenized measurements and (b) ERA5 reanalysis data.

entire period 1992–2020 has been considered for the comparison instead of the interval 2012–2020. Furthermore, as the MK4 test indicates a statistically significant trend in much more cases when compared to the MK3 test, the latter, which is a more conservative approach, has been used for the comparison presented in Figure 5.

An overall positive trend characterizes all seasons of the period 1969–1981 with the highest values exhibited by spring (1.034 m·s^{-1}/10 years, $p < 0.05$) and autumn (0.299 m·s^{-1}/10 years, $p > 0.10$), mainly due to the strong increasing trends observed in 2 of 3 months of each season: March and May on one side and September and October on the other side. On a monthly time scale, the strongest downward trend is encountered in February with −2.936 m·s^{-1}/10 years, followed by November with −2.872 m·s^{-1}/10 years and January with −1.026 m·s^{-1}/10 years, none of them statistically significant at the 0.10 level. The trend value for the winter season is however positive (0.097 m·s^{-1}/10 years, $p > 0.10$), due to the significant increasing trend exhibited by December (4.035 m·s^{-1}/10 years, $p < 0.10$), which is the second highest value over the 1969–1981 period, after that of March (7.538 m·s^{-1}/10 years, $p < 0.05$).

A pronounced gust speed decline is observed between 1992 and 2011 (Figure 5a). At the seasonal scale, decreasing tendencies are found in winter (−0.233 m·s^{-1}/10 years, $p > 0.10$) and spring (−0.038 m·s^{-1}/10 years, $p > 0.10$), whereas positive trends are observed in summer (0.285 m·s^{-1}/10 years, $p > 0.10$) and autumn (0.032 m·s^{-1}/10 years, $p > 0.10$), even though autumn shows lower magnitude value than for 1969–1981 period. Decreasing trends, almost unchanged compared to those of the period 1969–1981, continue to characterize the February (−2.741 m·s^{-1}/10 years, $p > 0.10$) and January (−0.846 m·s^{-1}/10 years, $p > 0.10$) time series. In addition to these, decreasing trends emerge in April (−2.171 m·s^{-1}/10 years, $p < 0.10$), June ($p > 0.10$), September and October. The highest increasing trends over the period 1992–2011 are encountered in July (3.760 m·s^{-1}/10 years) and November (1.679 m·s^{-1}/10 years), both statistically significant at $p < 0.05$.

A clear dominance of positive trends in gust speed emerges from Figure 5a over the period 1992–2020. Recovery of gust speed is particularly evident for winter, with significant positive trend of 0.329 m·s^{-1}/10 years ($p < 0.05$) over the mentioned period and 1.415 m·s^{-1}/10 years ($p < 0.10$) over the shorter interval 2012–2020. At the monthly time scale, February exhibits the strongest recovery, with an increasing trend of 1.489 m·s^{-1}/10 years ($p > 0.10$) over the period 1992–2020, after having showed the most marked negative trend in both intervals previously considered. The highest statistically significant ($p < 0.05$) positive trend over the period 1992–2020 is estimated for July with 1.937 m·s^{-1}/10 years, which is slightly lower than the 1992–2011 value due to modest monthly maximum gust speeds recorded in 2013, 2014, and 2016. Significant ($p < 0.05$) increasing

Table 4
Sen Slope Values Estimated for the Seasonal Time Series of the 1969–2014 Homogenized Monthly Maximum Gust Speeds in Order to Have Direct Comparison With European Existing Gust Trend Analyses (i.e., Azorin-Molina et al. (2016) and Brázdil et al. (2017))

	Sen slope ($m \cdot s^{-1}$/10 years)			
Series	MK1	MK2	MK3	MK4
DJF	−0.129	−0.109	**−0.129**	**−0.129***
MAM	0.171	0.147	0.171	**0.171***
JJA	**0.221***	**0.239***	**0.221***	**0.221***
SON	0.091	0.063	0.091	**0.091***

Note. Statistically significant trends at $p \leq 0.10$ level are indicated in bold and at $p \leq 0.05$ level in bold and with an asterisk.

trends are also encountered in November and December, with 1.859 and 1.537 $m \cdot s^{-1}$/10 years respectively, representing the second and third highest positive trends over the period 1992–2020.

A comparison has been performed with results of existing gust trend analyses in the European region. As shown in Table 4, agreement in trend sign is found with the winter decline observed over the period 1961–2014 in Czech Republic by Brázdil et al. (2017) (−0.784 $m \cdot s^{-1}$/10 years, estimated from their Table 2), and across Spain and Portugal by Azorin-Molina et al. (2016) (−0.168 $m \cdot s^{-1}$/10 years, $p < 0.10$, from their Table 2). Agreement in trend sign and significance (considering MK3 results) is also found with the increases in summer (0.148 $m \cdot s^{-1}$/10 years, $p < 0.05$) and autumn (0.041 $m \cdot s^{-1}$/10 years, not significant at $p < 0.10$) obtained by Azorin-Molina et al. (2016) for the 1961–2014 Spanish series. At the monthly time scale, the main difference in trend sign is given by the positive tendency detected at St Mary's in November and December over the period 1992–2011 and not observed in either Spanish or Czech time series. The most marked negative trend has been estimated in February at St Mary's and in the Iberian Peninsula (Azorin-Molina et al., 2016) and in November in Czech Republic (Brázdil et al., 2017).

4.3. Relationship With Air Temperature and Mean Sea Level Pressure Variations

The scatter plots in Figure 6 show the relationship between the monthly maximum gust speeds and the corresponding values of air temperature (left plot) and msl pressure (right plot) measured at St Mary's within a 6 hr time window centered on the gust occurrence time. A statistically significant ($p < 0.05$) negative correlation is found with both air temperature (−0.38) and msl pressure (−0.40). Therefore, changes in the pattern of mean air temperature and msl pressure have been examined in detail to assess their contribution to the observed gust speed variations.

Table 5 presents the estimates by using the HadUK-Grid monthly values of mean air temperature and msl pressure at St Mary's: their annual, seasonal and monthly trends as well as their Kendall correlation coefficients with the homogenized monthly maximum gust speeds. Despite considerable interannual variability, a statistically significant ($p < 0.05$) trend of 0.074°C/10 years is detected annually from the deseasonalized series of monthly mean air temperatures over the period 1884–2020. The estimated value is broadly consistent with the average rate of increase of 0.08°C/10 years since 1880 reported for the global average surface temperature by Sánchez-Lugo et al. (2021). A statistically significant positive trend is observed since 1884 across all seasons and months. Among the seasonal series, the greatest increases in mean temperature have been recorded in autumn (0.091°C/10 years) and spring (0.087°C/10 years), while winter shows the smallest identified increase (0.051°C/10 years). Among the monthly series, the largest warming trends have occurred in October, April, November and March.

Statistically significant negative correlations of similar magnitude are observed annually between the homogenized monthly maximum gust speeds and the corresponding monthly mean, minimum and maximum air

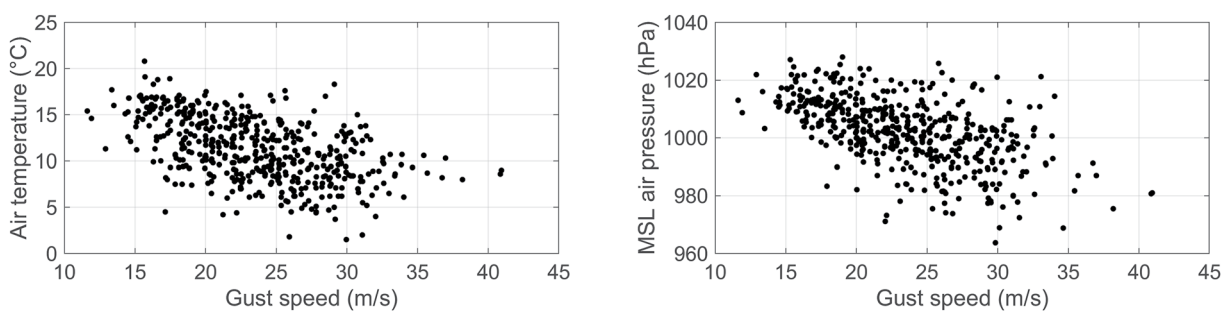

Figure 6. Monthly maximum gust speeds and corresponding values of air temperature (left plot) and mean sea level pressure (right) measured at St Mary's within a 6 hr time window centered on the gust occurrence time.

Table 5
Sen Slope Values Estimated for Mean Air Temperature (1884–2020) and msl Pressure (1961–2020) Using the HadUK-Grid Monthly Series and Correlation With the Monthly Maximum Gust Speeds From the Homogenized Measurements (τ_{Obs}) and ERA5 Reanalysis Data (τ_{ERA5}) Over the Period 1969–2020

	Mean air temperature							Mean sea level pressure						
	Sen slope (°C/10 years)							Sen slope (hPa/10 years)						
Series	MK1	MK2	MK3	MK4	MK5	τ_{Obs}	τ_{ERA5}	MK1	MK2	MK3	MK4	MK5	τ_{Obs}	τ_{ERA5}
Annual	**0.074***	**0.075***	**0.074***	**0.074***	**0.074***	**−0.42***	**−0.38***	−0.015	−0.016	**−0.015***	**−0.015**	−0.015	**−0.27***	**−0.27***
DJF	**0.051***	**0.051***	**0.051***	**0.051***	**0.051***	0.09	**0.15***	0.054	0.047	0.054	**0.054***	0.054	**−0.21***	**−0.24***
MAM	**0.087***	**0.089***	**0.087***	**0.087***	**0.087***	**−0.24***	**−0.30***	0.037	0.046	0.037	**0.037***	0.037	**−0.23***	**−0.25***
JJA	**0.069***	**0.069***	**0.069***	**0.069***	**0.069**	**−0.15***	**−0.09***	**−0.125***	**−0.125***	**−0.125***	**−0.125***	**−0.125***	**−0.33***	**−0.31***
SON	**0.091***	**0.092***	**0.091***	**0.091***	**0.091***	**−0.33***	**−0.27***	−0.020	−0.027	−0.020	−0.020	−0.020	**−0.33***	**−0.32***
January	**0.059***	**0.064***	**0.059***	**0.059***	**0.059***	0.08	**0.17***	0.612	0.513	0.612	**0.612***	0.612	**−0.19**	**−0.21***
February	**0.053**	**0.054***	**0.053**	**0.053***	**0.053**	−0.04	0.10	0.515	0.630	0.515	**0.515***	0.515	**−0.28***	**−0.28***
March	**0.079***	**0.081***	**0.079***	**0.079***	**0.079***	−0.01	−0.03	0.397	0.495	0.397	**0.397***	0.397	**−0.21***	**−0.21***
April	**0.092***	**0.091***	**0.092***	**0.092***	**0.092***	**−0.23***	−0.06	−0.111	−0.227	−0.111	−0.111	−0.111	**−0.36***	**−0.35***
May	**0.064***	**0.064***	**0.064***	**0.064***	**0.064***	0.08	**0.17***	0.195	0.258	0.195	**0.195***	0.195	**−0.19**	**−0.21***
June	**0.062***	**0.060***	**0.062***	**0.062***	**0.062***	**−0.24***	**−0.17***	−0.256	−0.184	−0.256	**−0.256***	−0.256	**−0.34***	**−0.34***
July	**0.067***	**0.067***	**0.067***	**0.067***	**0.067***	−0.15	**−0.20***	**−0.507***	**−0.526***	**−0.507***	**−0.507***	**−0.507***	**−0.34***	**−0.28***
August	**0.066***	**0.070***	**0.066***	**0.066***	**0.066***	**−0.31***	**−0.26***	−0.237	−0.228	−0.237	**−0.237***	−0.237	**−0.33***	**−0.29***
September	**0.068***	**0.071***	**0.068***	**0.068***	**0.068***	−0.12	−0.12	0.275	0.171	**0.275***	**0.275***	0.275	**−0.44***	**−0.38***
October	**0.107***	**0.103***	**0.107***	**0.107***	**0.107***	**−0.21**	−0.04	−0.523	**−0.709**	−0.523	**−0.523***	−0.523	**−0.26***	**−0.19***
November	**0.090***	**0.091***	**0.090***	**0.090***	**0.090***	−0.10	−0.08	−0.124	−0.222	−0.124	−0.124	−0.124	**−0.25***	**−0.30***
December	**0.059***	**0.058***	**0.059***	**0.059***	**0.059***	**0.19**	0.07	0.124	−0.003	0.124	0.124	0.124	−0.16	**−0.20***

Note. Statistically significant trends and correlation coefficients at $p \leq 0.10$ level are indicated in bold and at $p \leq 0.05$ level in bold and with an asterisk.

temperatures (Tables 5 and 6). At the seasonal scale, the highest significant ($p < 0.05$) correlations are obtained for autumn and spring.

A 30 years running trend analysis applied to the St Mary's deseasonalized monthly mean temperatures, whose results are shown in Figure 7, highlights the multi-decadal variability present in the long-term tendency. A comparison with the corresponding 30 years running trends calculated for the Santa Cruz de Tenerife and Valentia annual series is presented in Figure 7a. As already reported by Cropper and Hanna (2014), a shift of about 1°C is observed in the Santa Cruz temperature series. The shift is originated by a pronounced drop in the mean air temperature between 1991 and 1994, most likely related to the global cooling caused by the solar dimming due to the volcanic eruption of Mount Pinatubo (Luzon Island, Philippines) in June 1991 (Sanroma et al., 2010), which is followed by a rapid recovery between 1994 and 1999.

Negative trends are shown by the St Mary's annual series for the periods ranging from 1917 to 1936, intended as ending years of the corresponding rolling windows, with a minimum of −0.318°C/10 years in 1925. Negative running trends down to −0.111°C/10 years are found between 1968 and 1988. Two peaks are evident in the St Mary's series with positive trends of 0.289°C and 0.402°C/10 years in the ending years 1951 and 2007 respectively. An important acceleration in temperature increase emerges from the St Mary's data since the 1970s, consistent with the time of trend change in the global surface temperature outlined by Rahmstorf et al. (2017). From the 30 years running trends a reduced rate of warming is observed at St Mary's after 2007, which is only partially coinciding with the global warming slowdown period (2001–2014), mainly arising through the combined effects of internal decadal variability, volcanic and solar activity and decadal changes in anthropogenic aerosol forcing (Fyfe et al., 2016). After the value of 0.046°C/10 years estimated for the ending year 2018, progressively increasing running trends are obtained

Table 6
Kendall Correlation Coefficients Between the Homogenized Monthly Maximum Gust Speeds and the HadUK-Grid Monthly Minimum and Maximum Temperatures Over the Period 1969–2020

	Annual	DJF	MAM	JJA	SON
Minimum air temperature	**−0.40***	0.07	**−0.22***	−0.09	**−0.34***
Maximum air temperature	**−0.44***	**0.12***	**−0.28***	**−0.16***	**−0.32***

Note. Statistically significant correlation coefficients at $p \leq 0.10$ level are indicated in bold and at $p \leq 0.05$ level in bold and with an asterisk.

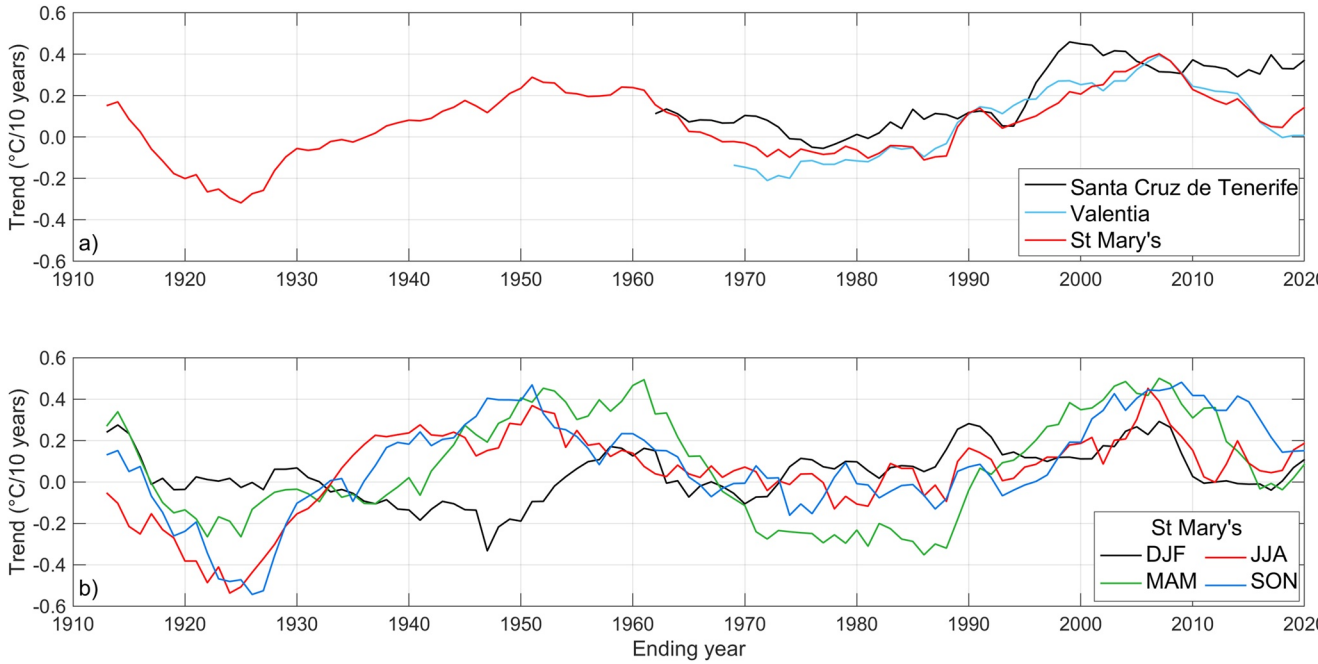

Figure 7. (a) 30 years running trends for the annual series of deseasonalized monthly mean air temperatures at St Mary's, Valentia and Santa Cruz de Tenerife. (b) 30 years running trends for the St Mary's seasonal series estimated from the deseasonalized monthly mean air temperatures.

for the two last periods analyzed, slightly greater than the corresponding 30 years running trends observed at the Valentia station (0.007°C/10 years).

The running trends for the St Mary's seasonal series are shown in Figure 7b. The spring, summer and autumn running trends fairly agree with the running trend of the annual series, while a more complex pattern is exhibited by the winter series.

The 30 years running trend analysis highlights a weakening of the air temperature gradient between the high and low latitudes from 1999 up to around the mid-2000s, in correspondence of rapidly increasing warming trends at the high latitudes. Since 2010, an increase of the air temperature gradient is observed concurrently with the slow-down in the surface warming rate at the high latitudes. This would suggest an important role of the strengthening of air temperature gradient between the high and low latitudes in the recent recovery of gust speed.

Considering the 1961–2020 deseasonalized monthly msl pressure values and the MK3 test results, statistically significant ($p < 0.05$) trends are found at St Mary's only for the annual series (−0.015 hPa/10 years), the summer period (−0.125 hPa/10 years) and, at the monthly time scale, for July (−0.507 hPa/10 years) and September (0.275 hPa/10 years) (Table 5).

A statistically significant negative correlation is observed between the monthly maximum gust speeds and the corresponding monthly values of msl pressure on annual basis (−0.27, $p < 0.05$) and, differently from mean air temperature, throughout all seasons (Table 5). Summer and autumn periods exhibit the highest negative correlation coefficient (−0.33), followed by spring (−0.23) and winter (−0.21). At the monthly time scale, the highest negative correlation coefficients are obtained for September, April and June ($p < 0.05$).

Figure 8 shows the results of a 15 years running trend analysis applied to the St Mary's deseasonalized monthly msl pressure values and a comparison with those obtained for Valentia and Santa Cruz. Positive running trends are detected in the St Mary's winter series over the periods 1982–1994 and 2005–2010, with maximum values of 0.772 and 0.840 hPa/10 years in 1992 and 2008 respectively. Limited negative running trends are observed in the St Mary's winter series between 1995 and 2004. A peak of 1.112 hPa/10 years is found in 1977 in the Santa Cruz winter running trends, while negative values are observed between 2002 and 2013. The important weakening of the latitudinal pressure gradient from the second half of the 1980s to 2004 and the 2005–2010 increased msl pressure at the high latitudes might have contributed to the decline of winter wind gusts observed at St Mary's. In

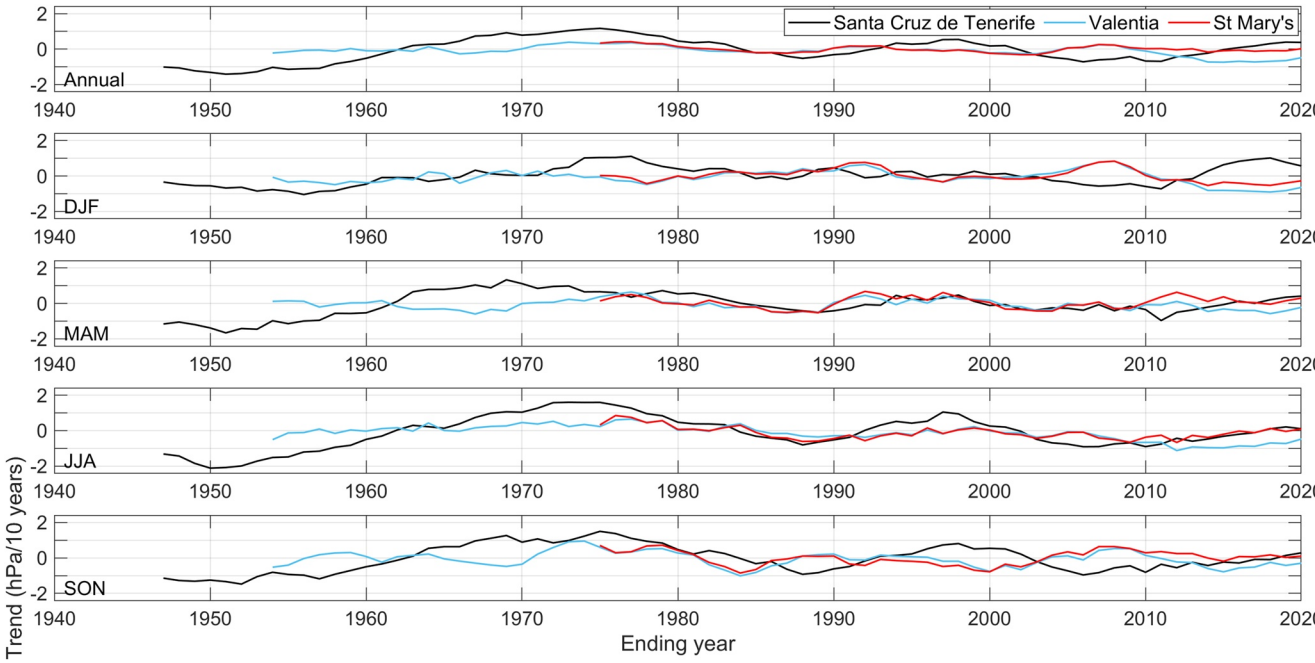

Figure 8. 15 years running trends for the annual and seasonal series of deseasonalized monthly msl pressure values at St Mary's, Valentia and Santa Cruz de Tenerife.

contrast, since 2014 positive running trends are detected in winter at Santa Cruz, while negative trends occur at St Mary's and, with more marked magnitude, at Valencia. The intensification of the latitudinal pressure gradient in recent years may have contributed to the recovery of winter gust speeds observed after 2012 (Figure 5a).

From Figure 8, a substantial reduction in the latitudinal pressure gradient is also evident in spring from the second half of the 1980s, which might have driven the observed decline in the gust speed at St Mary's in this season.

Two significant ($p < 0.05$) peaks are found in the summer running trends calculated from the Santa Cruz deseasonalized monthly msl pressure values: the first in 1975 with 1.593 hPa/10 years and the second in 1997 with 1.049 hPa/10 years. Between 2002 and 2017 negative trends in msl pressure are observed in summer at all three stations (Figure 8).

Two peaks are also found in the Santa Cruz autumn running trends, the first of 1.499 hPa/10 years in 1975 and the second of 0.809 hPa/10 years in 1998 (Figure 8). Increased pressure gradients are noted in autumn approximately between the mid-1990s and early 2000s. However, after 2004 positive running trends in msl pressure are observed at the high latitudes with likely effects on the autumn gust speeds at St Mary's.

Overall, the presented results highlight how the gust speed stilling observed at St Mary's and the more recent recovery are closely related to changes in the latitudinal pressure gradient. The gust speed reduction appears mainly due to a weakening of the pressure gradient between the high and low latitudes particularly in winter and spring. The gust speed increase observed in winter since 2012 appears to be consistent with the concurrent strengthening of the msl pressure gradient. These results are in agreement with previous studies of Yang et al. (2012) and Wu and Shi (2022), which highlighted the key role of pressure gradient in modulating the wind speed in China.

4.4. Comparison With the Maximum Gust Speeds From ERA5 Reanalysis

The estimated values for the Kendall and Pearson correlation coefficients between the homogenized monthly maximum gust speeds and the concurrent ERA5 values are 0.67 and 0.85 ($p < 0.05$) respectively. Root mean square error of 3.4 $m \cdot s^{-1}$ and bias equal to 1.8 $m \cdot s^{-1}$ are estimated between the homogenized and ERA5 data. There appears a general tendency by ERA5 to underestimate the magnitude of the actual monthly maximum gust events and to inaccurately capture the gust peak timing.

To remove the timing bias, the monthly maximum gust speeds identified in ERA5 output have been used to evaluate the performance of this reanalysis data set in simulating the observed gust variations at St Mary's. The temporal evolution of the ERA5 monthly maximum gust speeds is presented in Figure 4b. It is worth noting that the maximum value of 43.9 $m{\cdot}s^{-1}$ shown by the ERA5 reanalysis on 4 January 1998 at 10:00 does not represent the actual gust speed measured at St Mary's, where a maximum raw value of 35.5 $m{\cdot}s^{-1}$ was recored at 9:35, but rather the raw gust speed observed at the Culdrose station (42.1 $m{\cdot}s^{-1}$ at 11:50 and 12:51).

Even though the reanalysis data set seems to overall capture the decreasing trends of the monthly maximum gust speeds and the subsequent recovery, some substantial discrepancies are highlighted in the comparison with the tendencies of the homogenized measurements at St Mary's (Table 3 and Figure 5). Unlike the homogenized data, a pronounced negative trend is exhibited by the ERA5 July gust speeds in 1969–1981 (-2.541 $m{\cdot}s^{-1}$/10 years, $p > 0.10$), which drives the overall negative trend of the summer period over the same interval (-0.209 $m{\cdot}s^{-1}$/10 years, $p > 0.10$). Furthermore, during the period 1992–2011 the largest declining trend is found in April using the ERA5 data set (-3.024 $m{\cdot}s^{-1}$/10 years, $p < 0.10$) and not in February, as determined from the homogenized data. A strong decline is also found in October (-2.911 $m{\cdot}s^{-1}$/10 years, $p > 0.10$), which gives the major contribution to the relevant negative trend observed in the ERA5 autumn gust speeds (-0.155 $m{\cdot}s^{-1}$/10 years, $p > 0.10$). Moreover, a negative tendency is exhibited in 1992–2011 by the ERA5 December gust speeds (-0.468 $m{\cdot}s^{-1}$/10 years, $p > 0.10$), while a still positive trend is observed in the homogenized measurements (0.787 $m{\cdot}s^{-1}$/10 years, $p > 0.10$). Compared to the 1992–2020 seasonal trends of the homogenized maximum gust speeds, positive trends of lower magnitude are estimated for the ERA5 winter, summer and autumn gusts, while a weak negative tendency is exhibited by the ERA5 spring gusts (-0.011 $m{\cdot}s^{-1}$/10 years, $p > 0.10$), in contrast with the homogenized measurements (Figure 5).

The Kendall correlation coefficients between the ERA5 monthly maximum gust speeds and the corresponding St Mary's monthly msl pressures show similar values to those obtained for the homogenized measurements (Table 5). Some differences in magnitude and significance are revealed by the correlation coefficients estimated between the ERA5 monthly maximum gust speeds and the St Mary's monthly mean air temperatures, in comparison with the corresponding τ_{Obs}.

The identified discrepancies might be in part due to the coarse horizontal resolution of the ERA5 computational grid (31 km). The ERA5 limited spatial resolution may not accurately capture the wind variability and gust speeds in coastal areas due to the inherent sea-land roughness discontinuity (Gualtieri, 2021). Results of numerical experiments performed by using high-resolution simulations have shown to provide more detailed wind fields and higher and more realistic gust speeds compared with ERA5 reanalysis (Revokatova et al., 2021). A further limitation to exactly reproduce the gust speed trends on the monthly time scale may derive from the lack of assimilation of the observed land winds in ERA5. Comparison of reanalysis products shows that models assimilating land surface wind speeds can better simulate the spatiotemporal variations of the observed near-surface wind speeds (e.g., Shen et al., 2022).

4.5. Relationship With Large-Scale Climate Indices

Table 7 shows the annual, seasonal and monthly values of the Kendall correlation coefficient between the homogenized monthly maximum gust speeds at St Mary's and the considered 19 large-scale climate indices. To highlight the patterns with the greatest influence on the gust speed variations during the period 1969–2020, the magnitude of the trend of each climate index, evaluated in terms of seasonal means, is shown in Table 8.

The North Atlantic Oscillation (NAO) is the dominant mode of atmospheric circulation variability in the North Atlantic region, characterized by a north-south dipole structure with a low pressure center over Iceland (the Icelandic Low) and a high pressure center over the Azores (the Azores High). During positive NAO phases the Icelandic Low deepens and the Azores High strengthens increasing the msl pressure gradient over the North Atlantic and consequently enhancing the westerly winds over northern Europe (Hurrell, 1995). Conversely, during negative NAO phases a weakening of both the Icelandic Low and Azores High decreases the pressure gradient across the North Atlantic resulting in slackening of the westerly winds.

On annual scale weak positive correlation is found between the monthly maximum gust speeds and the station based CRU NAO (0.10, $p < 0.05$), while no correlation is observed with the CPC NAO. At the seasonal scale, a similar correlation value is found in winter for the CRU NAO (0.14, $p < 0.05$) and CPC NAO (0.16, $p < 0.05$),

Earth and Space Science

10.1029/2022EA002380

Table 7
Kendall Correlation Coefficient Between the Homogenized Monthly Maximum Gust Speeds and the Considered 19 Climate Indices

Climate index	Period	Annual	DJF	MAM	JJA	SON	January	February	March	April	May	June	July	August	September	October	November	December
CRU NAO	1969–2020	**0.10***	**0.14***	**0.11**	−0.07	0.02	0.12	−0.02	**0.20**	0.01	0.09	−0.03	**−0.19**	0.03	0.09	−0.00	−0.12	**0.34***
CPC NAO	1969–2020	−0.01	**0.16***	0.02	**−0.14***	**−0.14***	0.07	0.15	0.07	0.01	−0.03	**−0.19**	**−0.25***	−0.07	**−0.20**	−0.16	−0.07	**0.27***
SLP Val	1969–2016	**−0.23***	**−0.25***	**−0.26***	**−0.30***	**−0.30***	**−0.27***	**−0.24***	**−0.32***	**−0.36***	**−0.23**	**−0.29***	**−0.36***	**−0.36***	**−0.49***	**−0.31***	−0.16	**−0.22**
CPC EA	1969–2020	**0.12***	**0.15***	**0.20***	**0.26***	**0.16***	0.12	0.15	0.15	**0.25***	**0.21**	**0.35***	**0.19**	**0.33***	**0.25***	0.12	0.16	**0.23***
SLP Ber	1969–2017	**−0.23***	**−0.21***	**−0.33***	**−0.30***	**−0.30***	**−0.22***	−0.07	**−0.40***	**−0.43***	**−0.30***	**−0.38***	**−0.41***	−0.17	**−0.33***	**−0.37***	**−0.27***	**−0.30***
CPC SCA	1969–2020	0.04	0.08	−0.07	−0.08	**0.12***	0.16	0.04	−0.03	0.03	−0.11	**−0.19**	−0.02	−0.05	0.04	0.10	**0.24***	0.07
EA/WR	1969–2020	**−0.09***	−0.10	−0.07	−0.08	−0.05	−0.09	**−0.21**	−0.07	**−0.27***	−0.01	−0.07	**−0.20**	−0.01	0.02	−0.06	−0.17	−0.05
WEPA	1969–2018		**0.20***				**0.31***	**0.23***	**0.21**									0.02
TNH	1969–2020		**0.12***				−0.01	**0.20**										**0.20**
SOI	1969–2020	−0.03	**−0.16***	**−0.13***	−0.08	−0.01	**−0.25***	−0.15	**−0.18**	−0.15	−0.09	**−0.29***	0.13	−0.02	0.02	−0.00	−0.04	−0.06
AMM-SST	1969–2020	0.04	**−0.14***	−0.00	0.02	0.07	**−0.32***	−0.09	0.07	−0.11	−0.05	0.05	0.08	−0.13	−0.02	0.06	0.11	−0.09
AMM-wind	1969–2020	**−0.13***	**−0.18***	**−0.11**	0.01	**−0.15***	−0.11	−0.13	**−0.18**	**−0.21**	0.05	0.01	0.14	−0.08	−0.14	−0.10	−0.08	**−0.35***
ELI	1969-5/2020	**−0.15***	**0.18***	0.00	0.06	−0.09	**0.24***	0.13	0.09	0.02	−0.04	**0.24***	−0.06	−0.00	−0.09	0.15	0.03	0.17
Niño 3	1969–2020	0.04	**0.19***	0.04	0.04	0.03	**0.30***	0.08	0.06	0.09	0.02	**0.19**	−0.02	−0.02	−0.10	0.14	0.05	0.16
Niño 3.4	1969–2020	**0.07***	**0.18***	0.07	0.05	0.04	**0.28***	0.08	0.10	0.06	0.05	**0.20**	−0.02	0.00	−0.14	0.15	0.08	0.14
Niño 4	1969–2020	**0.09***	**0.18***	0.07	0.06	0.07	**0.25***	0.15	0.11	0.00	0.08	**0.18**	−0.02	0.04	−0.12	0.14	0.12	0.14
Niño 1+2	1969–2020	−0.01	**0.15***	−0.06	0.05	−0.03	**0.27***	0.03	−0.03	0.01	−0.14	0.16	−0.05	0.04	−0.07	0.03	−0.03	0.11
GLOTI	1969–2020	**0.11***	0.06	**0.15***	**0.20***	0.09	−0.03	0.09	0.12	0.09	0.16	**0.21**	**0.31***	0.15	−0.09	0.08	**0.30***	0.12
NHLOTI	1969–2020	**0.12***	0.06	**0.16***	**0.17***	**0.10**	−0.05	0.10	0.10	0.09	0.14	**0.19**	**0.23***	0.16	−0.02	0.03	**0.27***	0.15

Note. Statistically significant correlations at $p \leq 0.10$ level are indicated in bold and at $p \leq 0.05$ in bold and with an asterisk.

Table 8
Trends of the Climate Indices Considered in Terms of Seasonal Means Over the Period 1969–2020, Except for SLP Val (1969–2016), SLP Ber (1969–2017), WEPA (1969–2011) and ELI (1969–2019)

Climate index	DJF	MAM	JJA	SON
CRU NAO	**0.254***	0.145	**−0.255***	−0.120
CPC NAO	**0.213***	0.049	**−0.239***	−0.017
SLP Val	0.067	0.002	**−0.178***	**−0.105**
CPC EA	**0.187***	**0.178***	**0.353***	**0.220***
SLP Ber	−0.065	0.001	**−0.105**	0.056
CPC SCA	−0.067	**−0.199***	**−0.198***	0.087
EA/WR	−0.029	0.057	**−0.331***	**−0.189***
WEPA	**−0.200**			
TNH	**0.097***			
SOI	0.025	0.010	−0.049	0.010
AMM-SST	**0.577***	−0.048	0.200	**1.058***
AMM-wind	−0.539	0.399	**1.146***	**1.075***
ELI	−0.315	−0.345	−0.310	−0.286
Niño 3	0.013	**0.067***	**0.064**	0.002
Niño 3.4	−0.010	0.058	0.078	0.028
Niño 4	0.054	0.077	**0.118***	**0.112***
Niño 1+2	0.033	0.029	0.013	−0.030
GLOTI	**0.191***	**0.183***	**0.179***	**0.197***
NHLOTI	**0.272***	**0.265***	**0.237***	**0.273***

Note. The statistical significance of the trends has been estimated through the MK3 test. Statistically significant trends at $p \leq 0.10$ level are indicated in bold and at $p \leq 0.05$ level in bold and with an asterisk. Units are per decade.

while a statistically significant negative correlation is observed in summer only for the CPC NAO (−0.14, $p < 0.05$), reflecting the northward shift in the position of the southern NAO center in this season (Folland et al., 2009).

At the Isles of Scilly the gust speeds appear more affected by other leading modes of atmospheric variability, namely, the East Atlantic (EA) and Scandinavian (SCA) patterns. The EA pattern is the second prominent mode of climate variability in the North Atlantic region and appears as a leading mode in all months. According to Barnston and Livezey (1987), it is defined by a north-south dipole structure of geopotential height anomalies with a center located to the west of Ireland (55°N, 20°–35°W) and a band of opposite sign over the North Africa or the Mediterranean Sea (25°–35°N, 0°–10°W). Positive EA phases are associated with a negative pressure anomaly west of Ireland and a positive pressure anomaly over the subtropical North Atlantic, accompanied by southwesterly wind anomalies which bring warm air toward Europe. Negative EA phases are associated with an intense high pressure system over the midlatitude West Atlantic causing a northeasterly flow of cold, dry air from continental Europe over the Mediterranean region (Josey et al., 2011). The EA pattern identified by NOAA CPC (2021a), that is, CPC EA, is similar to that shown by Barnston and Livezey (1987). The instrumental EA pattern derived by Comas-Bru and Hernández (2018a), that is, SLP Val, is calculated through standardized sea level pressure anomalies from the measurements of the Valentia Observatory (Ireland) station. It is noted that the EA pattern considered by Comas-Bru and Hernández (2018a) is equivalent to the Atlantic Ridge regime (Comas-Bru & McDermott, 2014), therefore SLP Val has opposite sign compared to the CPC EA pattern (see Figure 3 in Comas-Bru & Hernández, 2018b).

The third leading mode of climate variability in the North Atlantic region, the SCA pattern, consists of a primary circulation center over the Scandinavian Peninsula, with weaker centers of opposite sign over western Europe and eastern Russia/western Mongolia. The positive phase of this pattern is characterized by positive geopotential height anomalies, sometimes reflecting major blocking anticyclones, over Scandinavia and western Russia (NOAA CPC, 2021d). During the positive phase, the North Atlantic storm-track activity weakens around Iceland and northern Europe, whereas the storm track extends eastwards into southern Europe through England (Bueh & Nakamura, 2007). The negative phase of the SCA pattern is associated with negative geopotential height anomalies over Scandinavia. Correspondingly, the Atlantic storm track extends north-eastwards and its activity enhances in a vast area from northern Europe to central Siberia.

As shown in Table 7, a strong significant negative correlation is obtained between the St Mary's monthly maximum gust speeds and SLP Val on annual scale and in all seasons, due to the proximity to the main center of action of the EA pattern. A significant positive correlation is found with the CPC EA on annual scale and in all seasons, consistent with that exhibited by SLP Val, although of slightly lower magnitude. The results show a strong significant negative correlation with SLP Ber almost throughout the year, except for February and August. On annual scale there is no correlation between the St Mary's monthly maximum gust speeds and CPC SCA, while on seasonal scale a significant correlation is only found in autumn and, moreover, with positive sign, in contrast with SLP Ber. As pointed out by Comas-Bru and Hernández (2018b), the SLP Val and SLP Ber station-based indices can be used as a reference in winter, when the atmosphere is most active dynamically and the two climate modes are more manifested, while they might not effectively represent the nonstationary behavior of the centers of action throughout the year, being anchored to fixed locations. However, the Kendall correlation coefficient value obtained between the St Mary's winter maximum gust speeds and SLP Ber (−0.23, $p < 0.05$) appears in line with the estimates given by Zubiate et al. (2017, see their Figure 5c).

Recent studies of Moore et al. (2013), Comas-Bru and McDermott (2014), and Zubiate et al. (2017) have highlighted that the EA and SCA patterns can modify the geographical location of the NAO dipole and modulate its

Table 9
Kendall Correlation Coefficient Between the St Mary's Winter Maximum Gust Speeds and the NAO Index for Different Combinations of the NAO–EA and NAO–SCA Phases

Series	Climate indices	NAO	NAO–EA same	NAO–EA opposite	NAO–SCA same	NAO–SCA opposite
DJF	CRU NAO, SLP Val and SLP Ber	**0.14*** (127)	**−0.22** (35)	**0.51*** (29)	−0.05 (16)	**0.29*** (46)

Note. Statistically significant correlations at $p \leq 0.10$ level are indicated in bold and at $p \leq 0.05$ level in bold and with an asterisk. The number of occurrences in months for each sign combination is shown in round brackets.

strength. In order to quantify the influence of the EA pattern on the correlation between the monthly maximum gust speeds and NAO at St Mary's, the winter data have been divided into two subsets characterized by NAO and EA patterns exhibiting the same phase (i.e., both indices greater than 0.5 or lesser than −0.5) or opposite phase. The same analysis has been performed to assess the SCA effect on the correlation between the monthly maximum gust speeds and NAO, following the approach of Comas-Bru and McDermott (2014) and Zubiate et al. (2017). The values of the Kendall correlation coefficient estimated for the different combinations of the NAO–EA and NAO–SCA phases are shown in Table 9.

The results presented in Table 9 show that the monthly maximum gust speeds at St Mary's are strongly influenced by the concomitant phase of the EA and SCA patterns. A significant negative correlation is found when the NAO and EA are in the same phase, and a strong significant positive correlation is observed for NAO–EA and NAO–SCA in opposite phases. The estimated values for the correlation coefficients are in agreement with the findings of Zubiate et al. (2017), highlighting that the anticyclonic ridge associated with the EA pattern contributes to weaken the airflow over western and middle Europe, attenuating the NAO effect during its positive phase.

From the long-term behavior of the indices presented in Figure 9, it can be noted that during the period from 1983 to 2004 the CRU NAO and SLP Val were both positive, while the SLP Ber was predominantly negative. According to Zubiate et al. (2017), this implies a northeastwards movement in the zero-line of the spatial correlation between the winter wind speed and NAO with respect to the general case and therefore a weakening of wind speeds in the southwestern part of England, in agreement with the observed decline in gust speed at St Mary's (as described in Section 4.2). Since 2012 the NAO and EA patterns exhibit opposite phase, as well as the NAO and SCA, resulting in enhanced wind speeds over the southwestern England. This is consistent with the observed recovery in wind gusts at St Mary's just since 2012.

The East Atlantic/West Russia (EA/WR) pattern consists of four main anomaly centers (Barnston & Livezey, 1987). In particular, the positive phase of the EA/WR pattern is characterized by positive geopotential height anomalies over Europe and northern China, and negative anomalies over the central North Atlantic and north of the Caspian Sea (NOAA CPC, 2021b). The EA/WR pattern is associated with circulation anomalies and temperature advection patterns that produce regions of alternating warm and cold (Lim, 2015). During the positive EA/WR phase, a strong anticyclonic circulation occurs over Europe and cyclonic over western Russia: these anomalies contribute to determine warm advection over the North-East Atlantic extending into western Europe (Lim, 2015). From

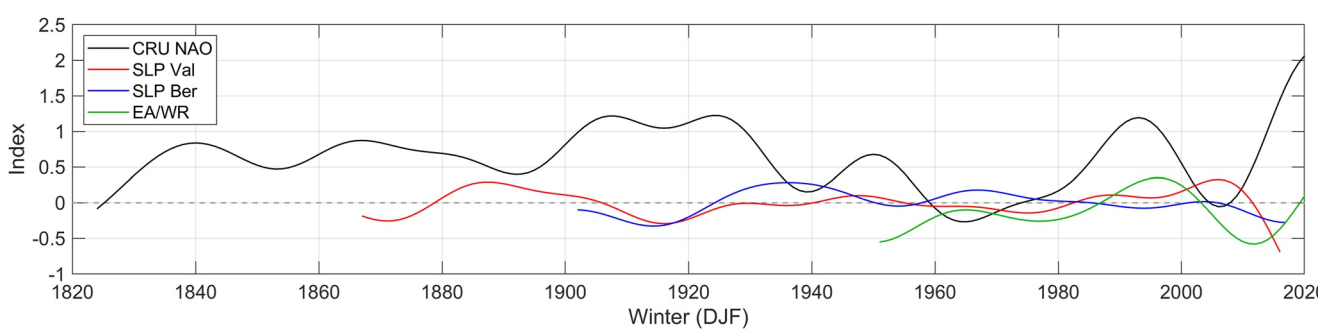

Figure 9. Winter mean (DJF) time series of CRU NAO (black curve), SLP Val (red curve), SLP Ber (blue curve) and EA/WR (green curve). The long-term behavior of the indices has been estimated through the procedure described by Mann (2008), using a 10 point Butterworth low-pass filter with cutoff frequency corresponding to a 21 year period.

Table 10
Kendall Correlation Coefficient Between the St Mary's Monthly Maximum Gust Speeds and the AMM Indices During the Periods 1971–1994 (P1) and 1995–2013 (P2)

AMM	Period	Ann	DJF	MAM	JJA	SON	January	February	March	April	May	June	July	August	September	October	November	December
SST	P1	0.01	−0.07	0.15	−0.01	−0.06	−0.03	−0.23	**0.49***	−0.03	0.08	0.01	0.27	−0.22	−0.11	0.15	−0.23	0.16
Wind	P1	−0.05	−0.08	0.08	−0.16	−0.14	−0.12	−0.10	−0.02	0.07	**0.38**	0.03	0.23	**−0.44***	**−0.36**	−0.09	0.02	0.03
SST	P2	**0.10***	−0.07	−0.05	0.05	0.07	**−0.42***	0.06	−0.01	−0.23	−0.07	0.06	0.12	−0.19	0.09	0.00	−0.10	−0.08
Wind	P2	**−0.19***	**−0.22***	**−0.25***	0.00	**−0.21***	−0.20	−0.02	−0.23	**−0.43***	−0.23	0.01	0.06	−0.12	0.04	−0.11	−0.19	**−0.52***

Note. Statistically significant correlations at $p \leq 0.10$ level are indicated in bold and at $p \leq 0.05$ level in bold and with an asterisk.

Table 7, a weak significant negative correlation is observed annually between the St Mary's monthly maximum gust speeds and the EA/WR pattern (−0.09, $p < 0.05$). No significant correlation emerges at the seasonal scale, even though significant negative correlations are observed in February (−0.21, $p < 0.10$), April (−0.27, $p < 0.05$) and July (−0.20, $p < 0.10$). From Figure 9, it can be noted that from approximately 1987 to 2003 the winter CRU NAO, SLP Val and EA/WR were all in their positive phase. However, the negligible trends obtained in winter and spring for EA/WR (Table 8) would suggest that this pattern had a minor influence on the gust speed variations observed at St Mary's in these two seasons.

The Western Europe Pressure Anomaly (WEPA) index is based on the normalized sea level pressure difference measured between the stations of Valentia and Santa Cruz de Tenerife. The positive WEPA phase reflects an intensified and southward shifted latitudinal sea level pressure gradient in the North-East Atlantic, associated with stronger than average SW to W winds across the middle latitudes, driving severe storms which funnel high energy waves toward the west coast of Europe south of 52°N (Castelle et al., 2017). As expected from the findings reported in Section 4.3, a significant positive correlation (0.20, $p < 0.05$) is observed between the winter maximum gust speeds and the WEPA index at St Mary's. The significant ($p < 0.10$) negative trend of WEPA during the 1969–2011 period appears to confirm that the winter gust decline observed at St Mary's is closely related to a weakening of the latitudinal pressure gradient.

The Atlantic Meridional Mode (AMM) represents the leading mode of coupled ocean-atmosphere variability in the Atlantic, and is significantly correlated with the Atlantic hurricane activity (Kossin & Vimont, 2007). The mode exhibits maximum variability in the boreal spring, but still retains substantial variability during the boreal summer Atlantic hurricane season (Kossin et al., 2010). Positive AMM phases, characterized by warm SST anomalies in the tropical North Atlantic and comparably cooler SSTs in the tropical South Atlantic, are associated with southwesterly wind anomalies in the tropical North Atlantic and northward migration of the Intertropical Convergence Zone (Rugg et al., 2016). Opposite conditions characterize the negative AMM phases. The AMM exhibits significant variability on interannual to decadal timescales. Positive AMM phases have been documented in 1925–1970 and after 1995, and a negative phase in 1971–1994 (Grossmann & Klotzbach, 2009).

From the Kendall correlation coefficients presented in Table 10, it can be noted that during the period 1971–1994 no statistically significant correlation is detected between the St Mary's monthly maximum gust speeds and the AMM indices neither on annual nor on seasonal scale. Conversely, during the period 1995–2013 characterized by a positive AMM phase, as shown in Figure 10, a statistically significant negative correlation is observed between the St Mary's monthly maximum gust speeds and the AMM-wind on annual scale and in winter, spring and autumn. During the period 1969–2013, the magnitude of the winter and spring AMM-wind trends, although statistically non-significant ($p > 0.10$), is markedly positive with rates of 0.187 and 0.690 $m \cdot s^{-1}$/10 years respectively, indicating that this mode, which reaches its peak in spring, likely contributed to the declining gust speed trends observed at St Mary's in these two seasons.

SST and surface wind stress anomalies in the central to eastern equatorial Pacific can result in warm (El Niño) and cold (La Niña) ENSO phases. From Table 7, it can be noted that a significant positive correlation is found between the magnitude of the St Mary's monthly maximum gust speeds and ENSO in winter, when most ENSO warm events reach their mature phase. In particular, the ENSO signal is most evident in January (0.24–0.30, $p < 0.05$). In the other seasons no clear El Niño signal appears in St Mary's gust speeds, even though a significant positive relationship is observed in June with ELI, Niño 3, Niño 3.4 and Niño 4 (0.18–0.24, $p < 0.10$). The estimated St Mary's gust speed trend would not seem to be significantly modulated by ENSO.

From Table 7, a weak statistically significant correlation (0.12, $p < 0.05$) is observed between the winter maximum gust speeds and the Tropical/Northern Hemisphere Pattern (TNH). Ayarzagüena et al. (2019) showed that some eastern Pacific El Niño signal reaches Europe through excitation of the TNH wavetrain in the month of February. Due to its tendency toward positive phases (Table 8), it is unlikely that this pattern was related to the gust decline detected in the St Mary's homogenized data.

The Southern Oscillation Index (SOI) is defined as the normalized msl pressure difference between Tahiti (French Polynesia) and Darwin (Australia), and is a measure of the large-scale fluctuations in air pressure occurring between the eastern and western tropical Pacific during El Niño and La Niña episodes. Specifically, a negative phase of the SOI indicates below-average air pressure at Tahiti and above-average air pressure at Darwin.

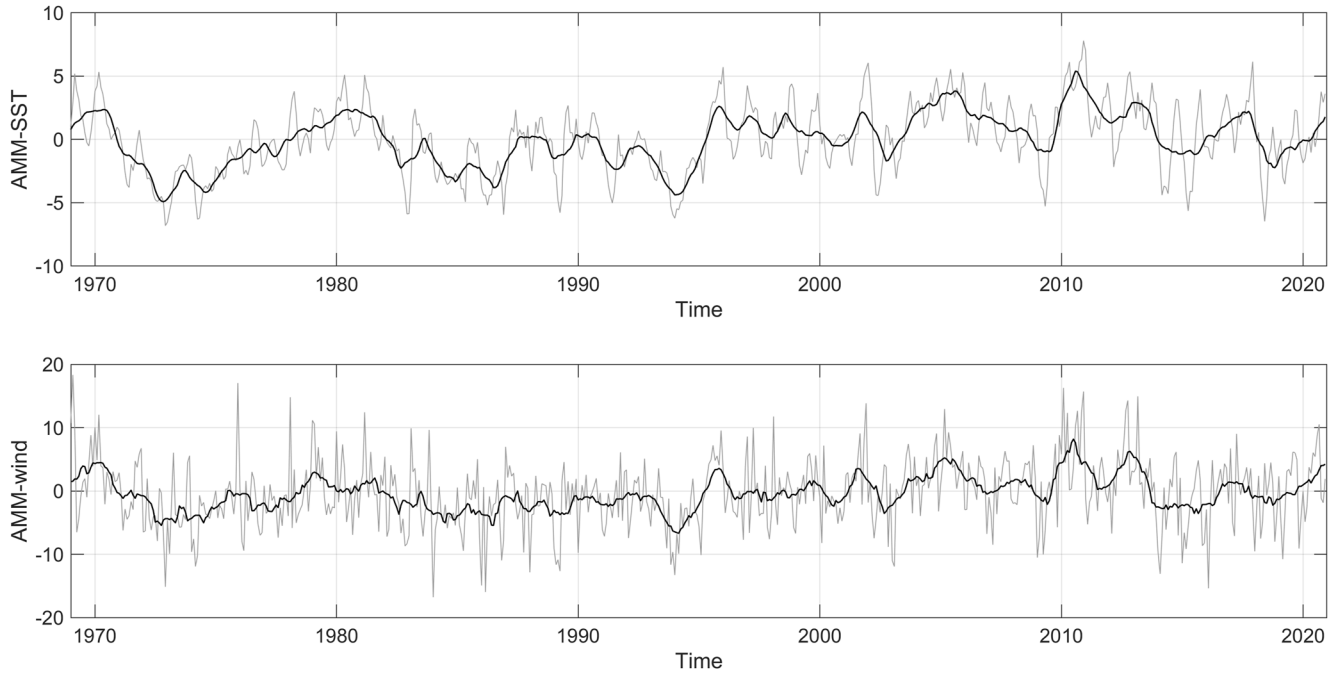

Figure 10. Time series of the Atlantic Meridional Mode (AMM)-sea surface temperature and AMM-wind monthly data (light gray line) and 12 months running mean (black line).

Prolonged periods of negative SOI values coincide with abnormally warm ocean waters across the eastern tropical Pacific, typical of El Niño episodes. Similarly, prolonged periods of positive SOI values coincide with La Niña events. Twelve El Niño events with SOI values below −1 occurred between 1972 and 2010, as shown in Figure 11. From Table 7, a statistically significant negative correlation is observed between the St Mary's monthly maximum gust speeds and SOI in winter (-0.16, $p < 0.05$) and spring (-0.13, $p < 0.05$). However, due to the lack of significant seasonal trends in SOI (Table 8), this pattern is unlikely to have driven the observed tendencies in St Mary's maximum gust speeds.

The Global Land-Ocean Temperature Index (GLOTI) is a measure of the anomaly in the global land-ocean temperature relative to the base period 1951–1980. It reflects anomalous warming since the early 1970s. A significant positive correlation is found between the St Mary's monthly maximum gust speeds and GLOTI at annual scale, and, on seasonal scale, in spring and summer (Table 7). Similar correlation values are obtained with NHLOTI, the Northern Hemisphere Land-Ocean Temperature Index. A weak significant positive correlation is also found in autumn (0.10, $p < 0.10$) with NHLOTI. On the monthly time scale, the highest significant ($p < 0.05$) correlation values are observed in July and November. The positive correlation between the maximum gust speeds and both these two indices, together with their significant positive trend (Table 8), would appear to

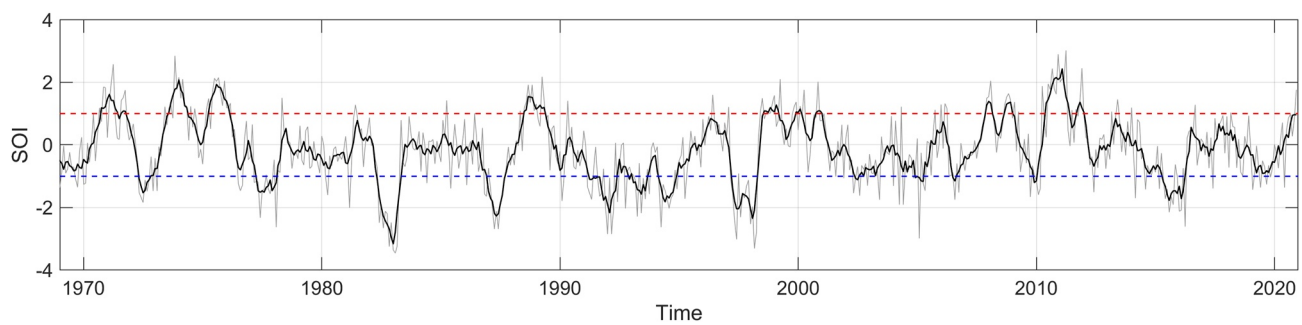

Figure 11. Time series of the Southern Oscillation Index monthly data (light gray line) and 5 months running mean (black line). The dashed blue line represents the El Niño event threshold, while the red dashed line marks the La Niña threshold.

suggest a contribution of the global warming to the observed increase in the summer gust speeds at St Mary's over the investigated period (Table 3 and Figure 5a).

5. Conclusions

In this study a rigorous homogenization procedure has been applied to the gust speeds recorded at St Mary's (Isles of Scilly) to remove inhomogeneities caused by non-climatic changes, mainly resulting from variations in the employed instrumentation, data acquisition practice, observation site and measurement height. Directional effective roughness lengths have been determined using the measured data to consider the effect of the surrounding terrain. Errors up to 12% would have been introduced in the subsequent analyses if the measured gust speeds had not been adjusted for differences in site exposure conditions. Trend analysis has been performed on the homogenized data.

The magnitude and sign of gust speed trend, as well as its statistical significance, are strongly dependent on the starting and ending dates of the observation interval considered. A statistically significant declining trend is observed in the annual maximum gust speeds during the period 1928–2011 (-0.102 m·s^{-1}/10 years, $p < 0.10$ for MK3), while a non-significant positive trend is found over the entire period of wind measurements 1928–2020. Considering the monthly maximum gust speeds, a statistically non-significant positive trend is observed annually over the period 1969–2011, while a significant increasing trend is estimated during 1969–2020 (0.157 m·s^{-1}/10 years, $p < 0.05$). A statistically significant turning point has been identified in the monthly maximum gust speed series in 2012, followed by a marked trend reversal.

Distinctive differences are observed among the seasons in the trend pattern of the monthly maximum gust speeds. Considering the period 1969–2011, a significant ($p < 0.05$) negative trend is found in winter, while a significant ($p < 0.10$ for MK3) positive trend is estimated for summer. A recovery of winter gust speed is observed since 2012, while a statistically significant ($p < 0.05$) positive trend is maintained by the summer gust speeds over the entire period 1969–2020.

Variations in the monthly maximum gust speeds appear closely related to changes in the air temperature and msl pressure gradients between the high and low latitudes. The 30 years running trend analysis for the annual series of monthly mean air temperatures highlights a reduction of the temperature gradient between the high and low latitudes from 1999 up to around the mid-2000s, in correspondence with increasing warming trends at the high latitudes. Since 2010 a strengthening of the temperature gradient is observed between the high and low latitudes concurrently with the slowdown in the surface warming at the high latitudes. The 15 years running trend analysis for the seasonal series of msl pressure highlights an important weakening of the latitudinal pressure gradient, particularly in winter and spring, which likely contributed to the observed decline in the gust speed at the study site. The recovery of winter gust speed since 2012 appears to be consistent with the concurrent strengthening of the latitudinal pressure gradient in this season.

Inaccurate estimates of magnitude and peak time are detected in the ERA5 monthly maximum gust speeds compared to the homogenized observations. Although ERA5 appears to capture the overall changes in the monthly maximum gust speeds, some substantial discrepancies are revealed by the comparison with the homogenized data. First of all, over the period 1992–2011 the largest declining trend in gust speed is found in April from the ERA5 data and not in February, as determined through the St Mary's measurements.

Changes in the main oceanic-atmospheric circulation patterns have a marked influence on the monthly maximum gust speeds at St Mary's. NAO–EA and NAO–SCA interactions appear to have contributed both to the observed decline in winter gust speeds and to the subsequent recovery after 2012. During its positive phase, the AMM-wind index, associated with tropical Atlantic climatic conditions, likely has contributed to the winter and spring decreasing gust speed trends observed at St Mary's. A significant correlation between the St Mary's monthly maximum gust speeds and ENSO signal is found in winter. However, ENSO does not appear to play a major role in modulating the gust speed trend. A statistically significant positive correlation is observed between the summer monthly maximum gust speeds and the GLOTI and NHLOTI indices, reflecting global and Northern Hemisphere warming trends.

Conflict of Interest

The authors declare no conflicts of interest relevant to this study.

Data Availability Statement

Wind and gust data used in the study were extracted upon request from the MIDAS Land and Marine Surface Stations data set, stored in the CEDA Archive: http://catalogue.ceda.ac.uk/uuid/220a65615218d5c9cc9e4785a3234bd0 (Met Office, 2012). For the reconstruction of the gust speed time series, data published in the Monthly Weather Reports were used: https://digital.nmla.metoffice.gov.uk/SO_47174b54-8030-4548-97cea2ff84349c7d/ (Met Office, 2021b). Gust speeds from the ERA5 reanalysis data were obtained through the ECMWF Copernicus Climate Change Service: http://climate.copernicus.eu/. Hourly data of air temperature and msl pressure at St Mary's were derived from http://dx.doi.org/10.5285/3bd7221d4844435dad2fa030f26ab5fd (Met Office, 2021a), whereas monthly values were extracted from the HadUK-Grid data set at http://dx.doi.org/10.5285/786b3ce6be54468496a3e11ce2f2669c (Met Office et al., 2021). Daily values of mean air temperature and msl pressure for the Valentia Observatory and Santa Cruz de Tenerife stations were derived through the website of the European Climate Assessment & Data set project: https://www.ecad.eu/ (Klein Tank et al., 2002); furthermore, for the Valentia station, data covering the period 30 May 2010 to 31 December 2020 were obtained from the Met Éireann website: https://www.met.ie/climate/available-data/historical-data. The time series of oceanic-atmospheric indices used in the study were freely retrieved from the sources specified in Table 1. The LiDAR data were derived from the UK Environment Agency through the open data portal https://environment.data.gov.uk/. The freely available R packages "RHtestsV4" (https://github.com/ECCC-CDAS/RHtests), "modifiedmk" (https://cran.r-project.org/web/packages/modifiedmk/index.html) and "HKprocess" (https://cran.r-project.org/web/packages/HKprocess/index.html) were used in the analyses.

Acknowledgments

The authors acknowledge the support of the EPSRC - EPSRC - Impact Accelerator Award, EP/V520342. The authors gratefully acknowledge the UK Met Office, the British Atmospheric Data Centre and the Centre for Environmental Data Analysis for providing access to the MIDAS data. The authors acknowledge the data providers in the ECA&D project. The authors warmly thank all agencies and research institutions mentioned in this study which provided free access to their data.

References

Aboshosha, H., Elawady, A., El Ansary, A., & El Damatty, A. (2016). Review on dynamic and quasi-static buffeting response of transmission lines under synoptic and non-synoptic winds. *Engineering Structures*, *112*, 23–46. https://doi.org/10.1016/j.engstruct.2016.01.003

Ambrose, J. (2021). Two UK energy suppliers collapse amid record surge in prices. *The Guardian*. Retrieved from https://www.theguardian.com/business/2021/sep/08/two-uk-energy-suppliers-succumb-to-record-surge-in-prices

Anderson, C. G. (2020). *Wind turbines: Theory and practice*. Cambridge University Press. https://doi.org/10.1017/9781108478328

Ayarzagüena, B., López-Parages, J., Iza, M., Calvo, N., & Rodríguez-Fonseca, B. (2019). Stratospheric role in interdecadal changes of El Niño impacts over Europe. *Climate Dynamics*, *52*(1), 1173–1186. https://doi.org/10.1007/s00382-018-4186-3

Azorin-Molina, C., Asin, J., McVicar, T. R., Minola, L., Lopez-Moreno, J. I., Vicente-Serrano, S. M., & Chen, D. (2018). Evaluating anemometer drift: A statistical approach to correct biases in wind speed measurement. *Atmospheric Research*, *203*, 175–188. https://doi.org/10.1016/j.atmosres.2017.12.010

Azorin-Molina, C., Guijarro, J.-A., McVicar, T. R., Vicente-Serrano, S. M., Chen, D., Jerez, S., & Espírito-Santo, F. (2016). Trends of daily peak wind gusts in Spain and Portugal, 1961–2014. *Journal of Geophysical Research: Atmospheres*, *121*(3), 1059–1078. https://doi.org/10.1002/2015JD024485

Azorin-Molina, C., McVicar, T. R., Guijarro, J. A., Trewin, B., Frost, A. J., Zhang, G., et al. (2021). A decline of observed daily peak wind gusts with distinct seasonality in Australia, 1941–2016. *Journal of Climate*, *34*(8), 3103–3127. https://doi.org/10.1175/JCLI-D-20-0590.1

Azorin-Molina, C., Rehman, S., Guijarro, J. A., McVicar, T. R., Minola, L., Chen, D., & Vicente-Serrano, S. M. (2018). Recent trends in wind speed across Saudi Arabia, 1978–2013: A break in the stilling. *International Journal of Climatology*, *38*(S1), e966–e984. https://doi.org/10.1002/joc.5423

Azorin-Molina, C., Vicente-Serrano, S. M., McVicar, T. R., Jerez, S., Sanchez-Lorenzo, A., López-Moreno, J.-I., et al. (2014). Homogenization and assessment of observed near-surface wind speed trends over Spain and Portugal, 1961–2011. *Journal of Climate*, *27*(10), 3692–3712. https://doi.org/10.1175/JCLI-D-13-00652.1

Bakker, F. P., & Viljoen, C. (2019). An analysis of South African wind gust data in the context of the built environment. In A. Zingoni (Ed.), *Advances in engineering materials, structures and systems: Innovations, mechanics and applications* (pp. 2352–2357). CRC Press/Balkema. https://doi.org/10.1201/9780429426506

Barnston, A. G., & Livezey, R. E. (1987). Classification, seasonality, and persistence of low-frequency atmospheric circulation patterns. *Monthly Weather Review*, *115*(6), 1083–1126. https://doi.org/10.1175/1520-0493(1987)115<1083:CSAPOL>2.0.CO;2

Bichet, A., Wild, M., Folini, D., & Schär, C. (2012). Causes for decadal variations of wind speed over land: Sensitivity studies with a global climate model. *Geophysical Research Letters*, *39*(11), L11701. https://doi.org/10.1029/2012GL051685

Blackall, R. M., Brown, R., & Collier, C. G. (1990). Real-time analysis of surface wind gusts using radar data: 25th January 1990. *The Meteorological Magazine*, *119*, 121–125.

Brázdil, R., Hostýnek, J., Řezníčková, L., Zahradníček, P., Tolasz, R., Dobrovolný, P., & Štěpánek, P. (2017). The variability of maximum wind gusts in the Czech Republic between 1961 and 2014. *International Journal of Climatology*, *37*(4), 1961–1978. https://doi.org/10.1002/joc.4827

Broomfield, C. S. (1982). Synoptic reports from the Isles of Scilly. *The Meteorological Magazine*, *111*, 185–189.

BSI. (2011). *BS EN 1991-1-4:2005+A1:2010. Eurocode 1: Actions on structures—Part 1-4: General actions—Wind actions*. British Standards Institution.

Bueh, C., & Nakamura, H. (2007). Scandinavian pattern and its climatic impact. *Quarterly Journal of the Royal Meteorological Society*, *133*(629), 2117–2131. https://doi.org/10.1002/qj.173

Castelle, B., Dodet, G., Masselink, G., & Scott, T. (2017). A new climate index controlling winter wave activity along the Atlantic coast of Europe: The West Europe Pressure Anomaly. *Geophysical Research Letters*, *44*(3), 1384–1392. https://doi.org/10.1002/2016GL072379

Cechet, R. P., & Sanabria, L. A. (2015). Statistical comparison of coincident wind gust measurements from Australian Dines and cup anemometers. In *Proceedings of the 14th International Conference on Wind Engineering, Porto Alegre, Brazil, 21–26 June 2015*.

Chen, T. Y. (1975). Comparison of surface winds in Hong Kong. Technical Note No. 41. Royal Observatory. Retrieved from https://www.hko.gov.hk/en/publica/tn/files/tn041.pdf

Comas-Bru, L., & Hernández, A. (2018a). Reconciling North Atlantic climate modes: Revised monthly indices for the East Atlantic and the Scandinavian patterns beyond the 20th century [Dataset]. PANGAEA. Retrieved from https://doi.org/10.1594/PANGAEA.892769

Comas-Bru, L., & Hernández, A. (2018b). Reconciling North Atlantic climate modes: Revised monthly indices for the East Atlantic and the Scandinavian patterns beyond the 20th century. *Earth System Science Data*, *10*(4), 2329–2344. https://doi.org/10.5194/essd-10-2329-2018

Comas-Bru, L., & McDermott, F. (2014). Impacts of the EA and SCA patterns on the European twentieth century NAO–winter climate relationship. *Quarterly Journal of the Royal Meteorological Society*, *140*(679), 354–363. https://doi.org/10.1002/qj.2158

Cook, N. (2007). *Designers' Guide to EN 1991-1-4. Eurocode 1: Actions on structures, general actions. Part 1-4: Wind actions*. Thomas Telford Limited.

Cook, N. J. (1985). *The designer's guide to wind loading of building structures—Part 1: Background, damage survey, wind data and structural classification*. Butterworths for Building Research Establishment, Department of the Environment.

Council of the Isles of Scilly. (2021). Isles of Scilly local plan 2015–2030. Retrieved from https://www.scilly.gov.uk/planning/planning-policy/local-plan-2015-2030

Cropper, T. E., & Hanna, E. (2014). An analysis of the climate of Macaronesia, 1865–2012. *International Journal of Climatology*, *34*(3), 604–622. https://doi.org/10.1002/joc.3710

CRU. (2021a). North Atlantic Oscillation (NAO) [Dataset]. Climatic Research Unit, University of East Anglia. Retrieved from https://crudata.uea.ac.uk/cru/data/nao/

CRU. (2021b). Southern Oscillation Index (SOI) [Dataset]. Climatic Research Unit, University of East Anglia. Retrieved from https://crudata.uea.ac.uk/cru/data/soi/

Dunn, R. J. H., Azorin-Molina, C., Mears, C. A., Berrisford, P., & McVicar, T. R. (2016). Surface winds [in "State of the Climate in 2015"]. *Bulletin of the American Meteorological Society*, *97*(8), S38–S40. https://doi.org/10.1175/2016BAMSStateoftheClimate.1

Earl, N., Dorling, S., Hewston, R., & von Glasow, R. (2013). 1980–2010 variability in U.K. surface wind climate. *Journal of Climate*, *26*(4), 1172–1191. https://doi.org/10.1175/JCLI-D-12-00026.1

Eden, P. (2008). *Great British weather disasters*. Continuum.

European Centre for Medium-Range Weather Forecasts (ECMWF). (2016). *IFS documentation Cy41r2—Part IV: Physical processes*. ECMWF. Retrieved from https://www.ecmwf.int/node/16648

Folland, C. K., Knight, J., Linderholm, H. W., Fereday, D., Ineson, S., & Hurrell, J. W. (2009). The summer North Atlantic Oscillation: Past, present, and future. *Journal of Climate*, *22*(5), 1082–1103. https://doi.org/10.1175/2008JCLI2459.1

Früh, W.-G. (2013). Long-term wind resource and uncertainty estimation using wind records from Scotland as example. *Renewable Energy*, *50*, 1014–1026. https://doi.org/10.1016/j.renene.2012.08.047

Fyfe, J. C., Meehl, G. A., England, M. H., Mann, M. E., Santer, B. D., Flato, G. M., et al. (2016). Making sense of the early-2000s warming slowdown. *Nature Climate Change*, *6*(3), 224–228. https://doi.org/10.1038/nclimate2938

Gardiner, B. (2021). Wind damage to forests and trees: A review with an emphasis on planted and managed forests. *Journal of Forest Research*, *26*(4), 248–266. https://doi.org/10.1080/13416979.2021.1940665

GCOS-WGSP. (2021a). Niño 1+2 SST Index [Dataset]. SystemWorking. Retrieved from https://www.psl.noaa.gov/gcos_wgsp/Timeseries/Nino12/

GCOS-WGSP. (2021b). Niño 3 SST Index [Dataset]. SystemWorking. Retrieved from https://www.psl.noaa.gov/gcos_wgsp/Timeseries/Nino3/

GCOS-WGSP. (2021c). Niño 3.4 SST Index [Dataset]. SystemWorking. Retrieved from https://www.psl.noaa.gov/gcos_wgsp/Timeseries/Nino34/

GCOS-WGSP. (2021d). Niño 4 SST Index [Dataset]. SystemWorking. Retrieved from https://www.psl.noaa.gov/gcos_wgsp/Timeseries/Nino4/

Gilbert, R. O. (1987). *Statistical methods for environmental pollution monitoring*. Van Nostrand Reinhold Company.

GISTEMP Team. (2021). GISS surface temperature analysis (GISTEMP), version 4 [Dataset]. NASA Goddard Institute for Space Studies. Retrieved from https://data.giss.nasa.gov/gistemp/

Grossmann, I., & Klotzbach, P. J. (2009). A review of North Atlantic modes of natural variability and their driving mechanisms. *Journal of Geophysical Research*, *114*(D24), D24107. https://doi.org/10.1029/2009JD012728

Gualtieri, G. (2021). Reliability of ERA5 reanalysis data for wind resource assessment: A comparison against tall towers. *Energies*, *14*(14), 4169. https://doi.org/10.3390/en14144169

Halliday, J. A. (1984). Analysis of wind speed data recorded at 14 widely dispersed U.K. meteorological stations. *Wind Engineering*, *8*(1), 50–73. Retrieved from http://www.jstor.org/stable/43749048

Hamed, K. H. (2008). Trend detection in hydrologic data: The Mann-Kendall trend test under the scaling hypothesis. *Journal of Hydrology*, *349*(3–4), 350–363. https://doi.org/10.1016/j.jhydrol.2007.11.009

Hamed, K. H., & Rao, A. R. (1998). A modified Mann-Kendall trend test for autocorrelated data. *Journal of Hydrology*, *204*(1–4), 182–196. https://doi.org/10.1016/S0022-1694(97)00125-X

Hersbach, H., Bell, B., Berrisford, P., Hirahara, S., Horányi, A., Muñoz-Sabater, J., et al. (2020). The ERA5 global reanalysis. *Quarterly Journal of the Royal Meteorological Society*, *146*(730), 1999–2049. https://doi.org/10.1002/qj.3803

Hewston, R., & Dorling, S. R. (2011). An analysis of observed daily maximum wind gusts in the UK. *Journal of Wind Engineering and Industrial Aerodynamics*, *99*(8), 845–856. https://doi.org/10.1016/j.jweia.2011.06.004

Hollis, D., McCarthy, M., Kendon, M., Legg, T., & Simpson, I. (2019). HadUK-Grid–A new UK dataset of gridded climate observations. *Geoscience Data Journal*, *6*(2), 151–159. https://doi.org/10.1002/gdj3.78

Holmes, J. D. (2015). *Wind loading of structures* (3rd ed.). CRC Press. https://doi.org/10.1201/b18029

Hooley, D. (2016). Shaping the Isles of Scilly, UK: The interplay of landscape and environment. In G. Pungetti (Ed.), *Island landscapes: An expression of European culture* (pp. 197–204). Routledge. https://doi.org/10.4324/9781315590110

Hu, L. (2017). A review of physics and correlations of pool fire behaviour in wind and future challenges. *Fire Safety Journal*, *91*, 41–55. https://doi.org/10.1016/j.firesaf.2017.05.008

Hurrell, J. W. (1995). Decadal trends in the North Atlantic Oscillation: Regional temperatures and precipitation. *Science*, *269*(5224), 676–679. https://doi.org/10.1126/science.269.5224.676

Irwin, P. A. (2006). Exposure categories and transitions for design wind loads. *Journal of Structural Engineering*, *132*(11), 1755–1763. https://doi.org/10.1061/(ASCE)0733-9445(2006)132:11(1755)

Josey, S. A., Somot, S., & Tsimplis, M. (2011). Impacts of atmospheric modes of variability on Mediterranean Sea surface heat exchange. *Journal of Geophysical Research*, *116*(C2), C02032. https://doi.org/10.1029/2010JC006685

Kendall, M. (1975). *Multivariate analysis*. Charles Griffin & Co. Ltd.

Kendall, M. G. (1970). *Rank correlation methods*. Charles Griffin & Co. Ltd.

Khosroshahi, S. F., Masina, M., Antonini, A., Ransley, E., Brownjohn, J. M. W., Dobson, P., & D'Ayala, D. (2022). A multidisciplinary computational framework for topology optimisation of Offshore Helidecks. *Journal of Marine Science and Engineering*, *10*(9), 1180. https://doi.org/10.3390/jmse10091180

Kim, J., & Paik, K. (2015). Recent recovery of surface wind speed after decadal decrease: A focus on South Korea. *Climate Dynamics*, *45*(5), 1699–1712. https://doi.org/10.1007/s00382-015-2546-9

Kirkham, G., Shepherd, F., & Johns, C. (2011). *Field boundaries on the Isles of Scilly: Historic environment study to inform management for conservation. Report No. 2011R095*. Historic Environment, Cornwall Council. https://doi.org/10.5284/1019238

Klein Tank, A. M. G., Wijngaard, J. B., Können, G. P., Böhm, R., Demarée, G., Gocheva, A., et al. (2002). Daily dataset of 20th-century surface air temperature and precipitation series for the European Climate Assessment. *International Journal of Climatology*, *22*(12), 1441–1453. https://doi.org/10.1002/joc.773

Kossin, J. P., Camargo, S. J., & Sitkowski, M. (2010). Climate modulation of North Atlantic hurricane tracks. *Journal of Climate*, *23*(11), 3057–3076. https://doi.org/10.1175/2010JCLI3497.1

Kossin, J. P., & Vimont, D. J. (2007). A more general framework for understanding Atlantic hurricane variability and trends. *Bulletin of the American Meteorological Society*, *88*(11), 1767–1782. https://doi.org/10.1175/BAMS-88-11-1767

Laapas, M., & Venäläinen, A. (2017). Homogenization and trend analysis of monthly mean and maximum wind speed time series in Finland, 1959–2015. *International Journal of Climatology*, *37*(14), 4803–4813. https://doi.org/10.1002/joc.5124

Lam, J. S. L., Liu, C., & Gou, X. (2017). Cyclone risk mapping for critical coastal infrastructure: Cases of East Asian seaports. *Ocean & Coastal Management*, *141*, 43–54. https://doi.org/10.1016/j.ocecoaman.2017.02.015

Li, C., Michel, C., Graff, L. S., Bethke, I., Zappa, G., Bracegirdle, T. J., et al. (2018). Midlatitude atmospheric circulation responses under 1.5 and 2.0°C warming and implications for regional impacts. *Earth System Dynamics*, *9*(2), 359–382. https://doi.org/10.5194/esd-9-359-2018

Lim, Y.-K. (2015). The East Atlantic/West Russia (EA/WR) teleconnection in the North Atlantic: Climate impact and relation to Rossby wave propagation. *Climate Dynamics*, *44*(11), 3211–3222. https://doi.org/10.1007/s00382-014-2381-4

Logue, J. J. (1986). Comparison of wind speeds recorded simultaneously by a pressure-tube anemograph and a cup-generator anemograph. *The Meteorological Magazine*, *115*, 178–185.

Logue, J. J. (1989). *The estimation of extreme wind speeds over standard terrain in Ireland. Technical Note No. 51*. Meteorological Service.

Lu, J., Vecchi, G. A., & Reichler, T. (2007). Expansion of the Hadley cell under global warming. *Geophysical Research Letters*, *34*(6), L06805. https://doi.org/10.1029/2006GL028443

Mann, H. B. (1945). Nonparametric tests against trend. *Econometrica*, *13*(3), 245–259. https://doi.org/10.2307/1907187

Mann, M. E. (2008). Smoothing of climate time series revisited. *Geophysical Research Letters*, *35*(16), L16708. https://doi.org/10.1029/2008GL034716

Masina, M., Lamberti, A., & Archetti, R. (2015). Coastal flooding: A copula based approach for estimating the joint probability of water levels and waves. *Coastal Engineering*, *97*, 37–52. https://doi.org/10.1016/j.coastaleng.2014.12.010

Masters, F. J., Vickery, P. J., Bacon, P., & Rappaport, E. N. (2010). Toward objective, standardized intensity estimates from surface wind speed observations. *Bulletin of the American Meteorological Society*, *91*(12), 1665–1682. https://doi.org/10.1175/2010BAMS2942.1

McCallum, E. (1990). The Burns' Day Storm, 25 January 1990. *Weather*, *45*(5), 166–173. https://doi.org/10.1002/j.1477-8696.1990.tb05607.x

McVicar, T. R., Roderick, M. L., Donohue, R. J., Li, L. T., Van Niel, T. G., Thomas, A., et al. (2012). Global review and synthesis of trends in observed terrestrial near-surface wind speeds: Implications for evaporation. *Journal of Hydrology*, *416–417*, 182–205. https://doi.org/10.1016/j.jhydrol.2011.10.024

McVicar, T. R., Van Niel, T. G., Li, L. T., Roderick, M. L., Rayner, D. P., Ricciardulli, L., & Donohue, R. J. (2008). Wind speed climatology and trends for Australia, 1975–2006: Capturing the stilling phenomenon and comparison with near-surface reanalysis output. *Geophysical Research Letters*, *35*(20), L20403. https://doi.org/10.1029/2008GL035627

McVicar, T. R., Van Niel, T. G., Roderick, M. L., Li, L. T., Mo, X. G., Zimmermann, N. E., & Schmatz, D. R. (2010). Observational evidence from two mountainous regions that near-surface wind speeds are declining more rapidly at higher elevations than lower elevations: 1960–2006. *Geophysical Research Letters*, *37*(6), L06402. https://doi.org/10.1029/2009GL042255

Menut, L. (2008). Sensitivity of hourly Saharan dust emissions to NCEP and ECMWF modeled wind speed. *Journal of Geophysical Research*, *113*(D16), D16201. https://doi.org/10.1029/2007JD009522

Meteorological Council. (1896). *Report of the Meteorological Council for the year ending 31st of March 1896; submitted to the President and Council of the Royal Society*. Eyre and Spottiswoode.

Met Office. (2012). Met Office Integrated Data Archive System (MIDAS) Land and Marine Surface Stations Data (1853-current) [Dataset]. NCAS British Atmospheric Data Centre. Retrieved from http://catalogue.ceda.ac.uk/uuid/220a65615218d5c9cc9e4785a3234bd0

Met Office. (2019). *Observational products—September 2019*. Met Office. Retrieved from https://www.metoffice.gov.uk/binaries/content/assets/metofficegovuk/pdf/data/uk_synop_station_list.pdf

Met Office. (2021a). MIDAS Open: UK hourly weather observation data, v202107 [Dataset]. NERC EDS Centre for Environmental Data Analysis. Retrieved from https://doi.org/10.5285/3bd7221d4844435dad2fa030f26ab5fd

Met Office. (2021b). *Monthly Weather Report*. Met Office Digital Library and Archive. Retrieved from https://digital.nmla.metoffice.gov.uk/SO_47174b54-8030-4548-97ce-a2ff84349c7d/

Met Office, Hollis, D., McCarthy, M., Kendon, M., Legg, T., & Simpson, I. (2021). HadUK-Grid Gridded Climate Observations on a 1 km grid over the UK, v1.0.3.0 (1862–2020) [Dataset]. NERC EDS Centre for Environmental Data Analysis. Retrieved from http://dx.doi.org/10.5285/786b3ce6be54468496a3e11ce2f2669c

Miller, C., Holmes, J., Henderson, D., Ginger, J., & Morrison, M. (2013). The response of the Dines anemometer to gusts and comparisons with cup anemometers. *Journal of Atmospheric and Oceanic Technology*, *30*(7), 1320–1336. https://doi.org/10.1175/JTECH-D-12-00109.1

Milne, R. (2021). Renewables leader Orsted hit by low wind speeds. *Financial Times*. Retrieved from https://www.ft.com/content/52c74f23-8bfc-44ac-bae8-663b369bd186

Minola, L., Azorin-Molina, C., & Chen, D. (2016). Homogenization and assessment of observed near-surface wind speed trends across Sweden, 1956–2013. *Journal of Climate*, *29*(20), 7397–7415. https://doi.org/10.1175/JCLI-D-15-0636.1

Minola, L., Reese, H., Lai, H.-W., Azorin-Molina, C., Guijarro, J. A., Son, S.-W., & Chen, D. (2022). Wind stilling-reversal across Sweden: The impact of land-use and large-scale atmospheric circulation changes. *International Journal of Climatology*, *42*(2), 1049–1071. https://doi.org/10.1002/joc.7289

Moore, G. W. K., Renfrew, I. A., & Pickart, R. S. (2013). Multidecadal mobility of the North Atlantic Oscillation. *Journal of Climate*, *26*(8), 2453–2466. https://doi.org/10.1175/JCLI-D-12-00023.1

Munich Re. (2002). *Winter storms in Europe (II): Analysis of 1999 losses and loss potentials*. Munich Re Group.

NOAA CPC. (2021a). East Atlantic (EA). [Dataset]. NOAA Climate Prediction Center. Retrieved from https://www.cpc.ncep.noaa.gov/data/teledoc/ea.shtml

NOAA CPC. (2021b). East Atlantic/Western Russia. [Dataset]. NOAA Climate Prediction Center. Retrieved from https://www.cpc.ncep.noaa.gov/data/teledoc/eawruss.shtml

NOAA CPC. (2021c). North Atlantic Oscillation (NAO). [Dataset]. NOAA Climate Prediction Center. Retrieved from https://www.cpc.ncep.noaa.gov/data/teledoc/nao.shtml

NOAA CPC. (2021d). Scandinavia (SCAND) [Dataset]. NOAA Climate Prediction Center. Retrieved from https://www.cpc.ncep.noaa.gov/data/teledoc/scand.shtml

NOAA CPC. (2021e). Tropical/Northern Hemisphere (TNH) [Dataset]. NOAA Climate Prediction Center. Retrieved from https://www.cpc.ncep.noaa.gov/data/teledoc/tnh.shtml

NOAA PSL. (2021). Monthly Climate Timeseries: Atlantic Meridional Mode (AMM) SST Index [Dataset]. NOAA Physical Sciences Laboratory. Retrieved from https://psl.noaa.gov/data/timeseries/monthly/AMM/

Pasquill, F. (1961). The estimation of the dispersion of windborne material. *The Meteorological Magazine*, *90*, 33–49.

Patakamuri, S. K., & O'Brien, N. (2021). modifiedmk: Modified versions of Mann Kendall and Spearman's rho trend tests. R package version 1.6 [Software]. CRAN. Retrieved from https://cran.r-project.org/web/packages/modifiedmk/index.html

Perry, A., & Symons, L. (1994). The wind hazard in the British Isles and its effects on transportation. *Journal of Transport Geography*, *2*(2), 122–130. https://doi.org/10.1016/0966-6923(94)90018-3

Petzold, J. (2017). *Social capital, resilience and adaptation on small islands: Climate change on the Isles of Scilly. Climate Change Management*. Springer International Publishing. https://doi.org/10.1007/978-3-319-52225-8

Pike, W. S. (1991). A further note on the severe storm of 25 January 1990. *The Journal of Meteorology*, *16*(155), 7–14.

Pirazzoli, P. A., Tomasin, A., & Ullmann, A. (2010). Recent changes in measured wind in the NE Atlantic and variability of correlation with NAO. *Annales Geophysicae*, *28*(10), 1923–1934. https://doi.org/10.5194/angeo-28-1923-2010

Rahmstorf, S., Foster, G., & Cahill, N. (2017). Global temperature evolution: Recent trends and some pitfalls. *Environmental Research Letters*, *12*(5), 054001. https://doi.org/10.1088/1748-9326/aa6825

Revokatova, A., Nikitin, M., Rivin, G., Rozinkina, I., Nikitin, A., & Tatarinovich, E. (2021). High-resolution simulation of polar lows over Norwegian and Barents Seas using the COSMO-CLM and ICON models for the 2019–2020 cold season. *Atmosphere*, *12*(2), 137. https://doi.org/10.3390/atmos12020137

Roderick, M. L., Rotstayn, L. D., Farquhar, G. D., & Hobbins, M. T. (2007). On the attribution of changing pan evaporation. *Geophysical Research Letters*, *34*(17), L17403. https://doi.org/10.1029/2007GL031166

Rugg, A., Foltz, G. R., & Perez, R. C. (2016). Role of mixed layer dynamics in tropical North Atlantic interannual sea surface temperature variability. *Journal of Climate*, *29*(22), 8083–8101. https://doi.org/10.1175/JCLI-D-15-0867.1

SA/SNZ (2011). AS/NZS 1170.2:2011. *Structural design actions. Part 2: Wind actions*. Standards Australia and Standards New Zealand.

Sánchez-Lugo, A., Morice, C., Nicolas, J. P., & Argüez, A. (2021). Global surface temperature [in "State of the Climate in 2020"]. *Bulletin of the American Meteorological Society*, *102*(8), S26–S28. https://doi.org/10.1175/BAMS-D-21-0098.1

Sanroma, E., Palle, E., & Sanchez-Lorenzo, A. (2010). Long-term changes in insolation and temperatures at different altitudes. *Environmental Research Letters*, *5*(2), 024006. https://doi.org/10.1088/1748-9326/5/2/024006

Scott, T., Masselink, G., Castelle, B., & Dodet, G. (2020). The West Europe Pressure Anomaly: 1943–2018 [Dataset]. University of Plymouth PEARL. Retrieved from http://hdl.handle.net/10026.1/15509

Sen, P. K. (1968). Estimates of the regression coefficient based on Kendall's tau. *Journal of the American Statistical Association*, *63*(324), 1379–1389. https://doi.org/10.1080/01621459.1968.10480934

Shen, C., Zha, J., Wu, J., Zhao, D., Azorin-Molina, C., Fan, W., & Yu, Y. (2022). Does CRA-40 outperform other reanalysis products in evaluating near-surface wind speed changes over China? *Atmospheric Research*, *266*, 105948. https://doi.org/10.1016/j.atmosres.2021.105948

Shu, Z. R., & Jesson, M. (2021). Estimation of Weibull parameters for wind energy analysis across the UK. *Journal of Renewable and Sustainable Energy*, *13*(2), 023303. https://doi.org/10.1063/5.0038001

Sloan, C., & Clark, M. R. (2012). A comparison of three Met Office wind observing systems. *Atmospheric Science Letters*, *13*(4), 283–288. https://doi.org/10.1002/asl.396

Spinoni, J., Formetta, G., Mentaschi, L., Forzieri, G., & Feyen, L. (2020). *Global warming and windstorm impacts in the EU. EUR 29960 EN*. Publications Office of the European Union. https://doi.org/10.2760/039014

Stephens, C. M., McVicar, T. R., Johnson, F. M., & Marshall, L. A. (2018). Revisiting pan evaporation trends in Australia a decade on. *Geophysical Research Letters*, *45*(20), 11164–11172. https://doi.org/10.1029/2018GL079332

Sunter, M. (2021). *MIDAS data user guide for UK land observations, v20210705*. Met Office. Retrieved from http://cedadocs.ceda.ac.uk/id/eprint/1492

Suomi, I., & Vihma, T. (2018). Wind gust measurement techniques–From traditional anemometry to new possibilities. *Sensors*, *18*(4), 1300. https://doi.org/10.3390/s18041300

Turner, R., Safaei Pirooz, A. A., Flay, R. G. J., Moore, S., & Revell, M. (2019). Use of high-resolution numerical models and statistical approaches to understand New Zealand historical wind speed and gust climatologies. *Journal of Applied Meteorology and Climatology*, *58*(6), 1195–1218. https://doi.org/10.1175/JAMC-D-18-0347.1

Tyralis, H. (2016). HKprocess: Hurst-Kolmogorov Process. R package version 0.0-2 [Software]. CRAN. Retrieved from https://cran.r-project.org/web/packages/HKprocess/index.html

Valta, H., Lehtonen, I., Laurila, T. K., Venäläinen, A., Laapas, M., & Gregow, H. (2019). Communicating the amount of windstorm induced forest damage by the maximum wind gust speed in Finland. *Advances in Science and Research*, *16*, 31–37. https://doi.org/10.5194/asr-16-31-2019

Vautard, R., Cattiaux, J., Yiou, P., Thépaut, J.-N., & Ciais, P. (2010). Northern Hemisphere atmospheric stilling partly attributed to an increase in surface roughness. *Nature Geosciences*, *3*(11), 756–761. https://doi.org/10.1038/ngeo979

Vose, R. S., Applequist, S., Bourassa, M. A., Pryor, S. C., Barthelmie, R. J., Blanton, B., et al. (2014). Monitoring and understanding changes in extremes: Extratropical storms, winds, and waves. *Bulletin of the American Meteorological Society*, *95*(3), 377–386. https://doi.org/10.1175/BAMS-D-12-00162.1

Wang, X. L., & Feng, Y. (2013). RHtestsV4 user manual. Climate Research Division, Atmospheric Science and Technology Directorate, Science and Technology Branch, Environment Canada. [Software]. Retrieved from https://github.com/ECCC-CDAS/RHtests

Watson, S. J., Kritharas, P., & Hodgson, G. J. (2015). Wind speed variability across the UK between 1957 and 2011. *Wind Energy*, *18*(1), 21–42. https://doi.org/10.1002/we.1679

Williams, I., & Patricola, C. (2020). ENSO Longitude Index (ELI) [Dataset]. Lawrence Berkeley National Laboratory. Retrieved from https://cascade.lbl.gov/enso-longitude-index-eli/

Wu, J., & Shi, Y. (2022). Changes in surface wind speed and its different grades over China during 1961–2020 based on a high-resolution dataset. *International Journal of Climatology*, *42*(7), 3954–3967. https://doi.org/10.1002/joc.7453

Wu, J., Zha, J., & Zhao, D. (2017). Evaluating the effects of land use and cover change on the decrease of surface wind speed over China in recent 30 years using a statistical downscaling method. *Climate Dynamics*, *48*(1), 131–149. https://doi.org/10.1007/s00382-016-3065-z

Wu, J., Zha, J., Zhao, D., & Yang, Q. (2018). Changes in terrestrial near-surface wind speed and their possible causes: An overview. *Climate Dynamics*, *51*(5), 2039–2078. https://doi.org/10.1007/s00382-017-3997-y

Yang, J., Shi, B., Shi, Y., Marvin, S., Zheng, Y., & Xia, G. (2020). Air pollution dispersal in high density urban areas: Research on the triadic relation of wind, air pollution, and urban form. *Sustainable Cities and Society*, *54*, 101941. https://doi.org/10.1016/j.scs.2019.101941

Yang, X., Li, Z., Feng, Q., He, Y., An, W., Zhang, W., et al. (2012). The decreasing wind speed in southwestern China during 1969–2009, and possible causes. *Quaternary International*, *263*, 71–84. https://doi.org/10.1016/j.quaint.2012.02.020

Young, I. R., & Ribal, A. (2019). Multiplatform evaluation of global trends in wind speed and wave height. *Science*, *364*(6440), 548–552. https://doi.org/10.1126/science.aav9527

Yue, S., Pilon, P., Phinney, B., & Cavadias, G. (2002). The influence of autocorrelation on the ability to detect trend in hydrological series. *Hydrological Processes*, *16*(9), 1807–1829. https://doi.org/10.1002/hyp.1095

Yue, S., & Wang, C. (2004). The Mann-Kendall test modified by effective sample size to detect trend in serially correlated hydrological series. *Water Resources Management*, *18*(3), 201–218. https://doi.org/10.1023/B:WARM.0000043140.61082.60

Zeng, Z., Ziegler, A. D., Searchinger, T., Yang, L., Chen, A., Ju, K., et al. (2019). A reversal in global terrestrial stilling and its implications for wind energy production. *Nature Climate Change*, *9*(12), 979–985. https://doi.org/10.1038/s41558-019-0622-6

Zha, J., Zhao, D., Wu, J., & Shen, C. (2021). Terrestrial near-surface wind speed variations in China: Research progress and prospects. *Journal of Meteorological Research*, *35*(3), 537–556. https://doi.org/10.1007/s13351-021-0143-x

Zhang, G., Azorin-Molina, C., Shi, P., Lin, D., Guijarro, J. A., Kong, F., & Chen, D. (2019). Impact of near-surface wind speed variability on wind erosion in the eastern agro-pastoral transitional zone of Northern China, 1982–2016. *Agricultural and Forest Meteorology*, *271*, 102–115. https://doi.org/10.1016/j.agrformet.2019.02.039

Zhou, L., Zeng, Z., Azorin-Molina, C., Liu, Y., Wu, J., Wang, D., et al. (2021). A continuous decline of global seasonal wind speed range over land since 1980. *Journal of Climate*, *34*(23), 9443–9461. https://doi.org/10.1175/JCLI-D-21-0112.1

Zubiate, L., McDermott, F., Sweeney, C., & O'Malley, M. (2017). Spatial variability in winter NAO–wind speed relationships in western Europe linked to concomitant states of the East Atlantic and Scandinavian patterns. *Quarterly Journal of the Royal Meteorological Society*, *143*(702), 552–562. https://doi.org/10.1002/qj.2943